Lawrence Berkeley National Laboratory
LBL Publications

Title

Hydrologic Characterization of Heterogeneous Geologic Media with an Inverse Method Based on Iterated Function Systems

Permalink

https://escholarship.org/uc/item/26m8h7sh

Journal

Water Resources Research, 30(6)

Authors

Doughty, Christine
Long, Jane C. S.
Kevin
et al.

Publication Date

1993-08-01

eScholarship.org Powered by the California Digital Library
University of California

LBL-34595
UC-403
Preprint

Lawrence Berkeley Laboratory

UNIVERSITY OF CALIFORNIA

EARTH SCIENCES DIVISION

Submitted to Water Resources Research

Hydrologic Characterization of Heterogeneous Geologic Media with an Inverse Method Based on Iterated Function Systems

C. Doughty, J.C.S. Long, K. Hestir, and S.M. Benson

August 1993

REFERENCE COPY
Does Not
Circulate
Bldg. 50 Library.
LBL-34595
Copy 1

Prepared for the U.S. Department of Energy under Contract Number DE-AC03-76SF00098

DISCLAIMER

This document was prepared as an account of work sponsored by the United States Government. While this document is believed to contain correct information, neither the United States Government nor any agency thereof, nor the Regents of the University of California, nor any of their employees, makes any warranty, express or implied, or assumes any legal responsibility for the accuracy, completeness, or usefulness of any information, apparatus, product, or process disclosed, or represents that its use would not infringe privately owned rights. Reference herein to any specific commercial product, process, or service by its trade name, trademark, manufacturer, or otherwise, does not necessarily constitute or imply its endorsement, recommendation, or favoring by the United States Government or any agency thereof, or the Regents of the University of California. The views and opinions of authors expressed herein do not necessarily state or reflect those of the United States Government or any agency thereof or the Regents of the University of California.

LBL-34595

Hydrologic Characterization of Heterogeneous Geologic Media with an Inverse Method Based on Iterated Function Systems

C. Doughty, J. C. S. Long, K. Hestir, and S. M. Benson

Earth Sciences Division
Lawrence Berkeley Laboratory
University of California
Berkeley, California 94720

August 1993

This work was supported by the Director, Office of Energy Research, Office of Health and Environmental Research, Subsurface Science Program, of the U.S. Department of Energy under Contract No. DE-AC03-76SF00098.

Hydrologic Characterization of Heterogeneous Geologic Media with an Inverse Method Based on Iterated Function Systems

Christine Doughty, Jane C.S. Long, Kevin Hestir,[1] and Sally M. Benson

Earth Sciences Division
Lawrence Berkeley Laboratory
University of California, Berkeley

August 1993

ABSTRACT

One way to estimate the hydrologic properties of heterogeneous geologic media is to invert well-test data using multiple observation wells. Pressure transients observed during a well test are compared to the corresponding values obtained by numerically simulating the test using a mathematical model. The parameters of the mathematical model are varied and the simulation repeated until a satisfactory match to the observed pressure transients is obtained, at which point the model parameters are accepted as providing a possible representation of the hydrologic property distribution. Restricting the search to parameters that represent self-similar (fractal) hydrologic property distributions can improve the inversion process. Far fewer parameters are needed to describe a hierarchical medium, improving the efficiency and robustness of the inversion. Additionally, each parameter set produces a hydrologic property distribution with a hierarchical structure, as is often seen in natural geological media. The parameters varied during the inversion create fractal sets known as attractors, using an iterated function system (IFS). An attractor is mapped to a distribution of transmissivity and storativity in the mathematical model. Thus the IFS inverse method searches for the parameters of the IFS (typically 10's of parameters) rather than the values of the hydrologic property distribution directly (typically 100's to 1000's of parameters). Application of the IFS inverse method to synthetic data shows that the method works well for simple heterogeneities. Application to field data from a sand/clay sedimentary sequence and a fractured granite produces reasonable results.

[1]Also at Department of Mathematics and Statistics, Utah State University, Logan

INTRODUCTION

MOTIVATION

An understanding of fluid flow and solute transport through porous or fractured geological media is necessary to address many current environmental problems, such as toxic chemical spills, leaking gasoline storage tanks, and long-term radioactive waste disposal, as well as to optimize energy extraction from petroleum or geothermal reservoirs. Mathematical modeling of the flow and transport processes is one means to gain such understanding. For realistic modeling, a description of the spatial distribution of the hydrologic properties of the medium (i.e., a hydrologic model) is needed, but the restricted view of the subsurface available through boreholes coupled with the extremely heterogeneous nature of most geologic media makes this difficult to obtain.

With the widespread use of computers over the past twenty years, numerous techniques for characterizing heterogeneous hydrologic property distributions have been developed. These techniques can be broadly divided into two groups, depending on whether they use a forward or inverse approach. In the forward approach, the hydrologic model is developed using information gained from basic studies of the site, including geological observations and geochemical, geophysical, petrophysical measurements. In the inverse approach, the general form of the hydrologic model is specified *a priori*, based on information from these basic studies, but the details of the model are determined by matching the predictions of the model to observed hydrologic behavior. Although both methods have advantages, each has drawbacks as well. In the present approach we try to incorporate some of the strengths of a geologically-based forward approach within the context of an inverse method.

ALTERNATIVE APPROACHES FOR CHARACTERIZATION OF HETEROGENEOUS MEDIA

In principle, any hydrologic model that contains adjustable parameters can be incorporated into an inverse method. A series of forward simulations are made with the model using different parameter values, then results of each simulation are compared to field observations. Parameters are chosen which give the best match between simulated and observed data. In practice, some models are more amenable to this process than others. In the paragraphs below, we outline several forward approaches to developing hydrologic models of heterogeneous geologic media and discuss their suitability for inclusion in an inverse method. Following this, we discuss some of the inherent strengths and weaknesses of the inversion of hydrologic data.

Before the widespread use of computers made numerical methods practical for solving subsurface fluid flow and solute transport problems, a vast number of analytical solutions were developed and adapted from other disciplines. With only a few parameters and very short times required for calculation, analytical solutions are well suited to inversion. However, the heterogeneities that can be treated with analytical solutions are limited to geometrically regular features such as linear vertical boundaries, horizontally layered media, and equally spaced fractures. Such simple geometries can only represent highly idealized models of geological media; to solve problems with heterogeneities that resemble the geometric irregularity observed in the field, numerical modeling is needed.

In a numerical model of a geologic medium, space can be discretized into irregularly shaped regions with different hydrologic properties. Both the number of parameters to be determined and the computational time for each forward simulation of the model increases drastically (typically by several orders of magnitude) compared to inversions using analytical solutions. Hence, inverse methods based on numerical forward calculations must be carefully designed to make use of computer time efficiently. The multiplicity of scales on which heterogeneities are observed in the field complicates the discretization, and at some scale heterogeneities cannot be treated individually but must be modeled as an effective medium. In an effective medium approach, a homogeneous region is used to represent a heterogeneous one by assigning hydrologic properties that incorporate the effects of the heterogeneities. The level of discretization needed depends on the amount of heterogeneity present and the problem at hand.

In contrast to the deterministic treatment of heterogeneities based on large-scale geological observations described above (e.g., clay layer overlying aquifer, permeable fracture zone separating intact blocks of low-permeability rock), geostatistics provides an alternate way to construct a hydrologic model. In geostatistics, the spatial distributions of hydrologic properties are described as spatially correlated random fields. A large number of (usually small-scale) measurements are made to determine the statistics of the distributions of the random fields, then a hydrologic model is constructed by drawing a realization from the distributions. For incorporation into an inverse method, geostatistics has the advantage that relatively few parameters need to be determined [*Kitanidis and Vomvoris*, 1983]. A disadvantage is that the small scale features being measured may not be relevant for large-scale flow, or may have an unknown cumulative response.

Another basis for creating a hydrologic model is to model the mechanisms involved in the creation of the geological medium, rather than to merely make observations or measurements of

the medium itself. Such mechanistic models are generally very computationally intensive [e.g., *Koltermann and Gorelick*, 1992], making them ill-suited to incorporation in a hydrologic inversion in which the forward model must be run many times. Recently however, several investigators have developed inexpensive mechanistic-based models by retaining only the key aspects of the physical mechanisms in a simple statistical way [*Long et al.*, 1993; *Webb*, 1992]. Such models would be amenable to incorporation in an inverse method by creating a series of realizations of the physical process, and testing each one to see how well it reproduces the hydrologic behavior. An optimization process would therefore find realizations which both match the hydrologic data and honor the physical process.

The principle advantage of using hydrologic inverse methods is that field-scale fluid flow (the well test) is used to develop a model that will ultimately be used to predict field-scale fluid flow (contaminant clean-up, geothermal fluid production, etc.), rather than observing another parameter such as geological facies or seismic-wave velocity and attempting to relate it to permeability. The method inherently emphasizes features that are important for flow and disregards the rest. In effect we develop equivalent media that do not have all the details of reality, but produce the same hydrologic response.

The principle disadvantage of using inverse methods for hydrologic characterization is that the fluid flow equation is a diffusion equation, and as such cannot be uniquely inverted to determine model parameters. One way to address non-uniqueness is to condition the inversion on additional information, such as prior estimates of model parameters [*Carrera and Neuman*, 1986a, 1986b, 1986c] or other geological or geophysical observations. Another approach is to do multiple inversions and study the statistics of the ensemble of results, such as the mean permeability distribution and its variance. A further practical disadvantage is that inverse methods tend to be computationally intensive, effectively precluding use of very complicated forward models. This should not be considered a fundamental limitation of the method, however, as rapid developments in both computer hardware and software make more and more complicated forward models usable in inverse methods.

THE PRESENT APPROACH

Our approach to the hydrologic characterization of heterogeneous geologic media involves the inversion of well-test data, because we believe using flow information to create a model that will ultimately be used to predict flow is a powerful technique. A numerical model is used to calculate head distribution and fluid flow in the forward problem. The model parameters that are

varied during the inversion determine the spatial variation of hydrologic properties. We restrict the search for model parameters to those which represent self-similar (or hierarchical) hydrologic property distributions. Thus we specify the nature of the overall geometry of the hydrologic property distribution, not the detailed physical processes leading to its formation.

The model parameters considered during the inversion process are generated using an iterated function system (IFS). The IFS's we use are composed of two to four affine transforms. An affine transform is a function which may rotate, reflect, deform, contract, and translate a set of points. When multiple transforms are applied iteratively, a set of points with a fractal geometry, known as an attractor, results. The attractor can be mapped to a distribution of transmissivity or storativity in a mathematical model. We then use the mathematical model to simulate the well test and compare the calculated heads to those observed during the test. If the match is not satisfactory, the parameters of the IFS are varied, and the simulation is repeated. This procedure continues until the IFS creates an attractor which yields a hydrologic property distribution that produces a good match to observed heads. A variety of optimization algorithms may be used to vary the parameters of the IFS during the course of the inversion; we primarily use one known as simulated annealing.

One of the primary strengths of the IFS inversion compared to other inverse methods is that far fewer parameters are needed to describe a self-similar medium than a medium with unstructured heterogeneities, making the inversion more efficient and more robust. Equally important is that the final parameter set produces a hydrologic property distribution with a hierarchical structure, as is often seen in natural geological media. In fact, by limiting the variation of parameters of the IFS, we can restrict the shape of the trial attractors to resemble observed hydrogeological features.

In the sections that follow, we first present the mathematical basis of IFS's and describe some practical features of the IFS inversion method. We then apply the method to synthetic data to study its strengths and weaknesses, and to field data from a sand/clay sedimentary sequence and a fractured granite.

$$|B_{11}| + |B_{12}| < 1 \tag{7}$$

$$|B_{21}| + |B_{22}| < 1 .$$

For convenience, we then restrict **b** so that the attractor is confined to the unit square $0 < x < 1$, $0 < y < 1$. The constraints on $\mathbf{b} = (b_1, b_2)$ depend on the entries of $\mathbf{B}$, and may be written as

$$-\min(0, B_{11}) - \min(0, B_{12}) < b_1 < 1 - \max(0, B_{11}) - \max(0, B_{12}) \tag{8}$$

$$-\min(0, B_{21}) - \min(0, B_{22}) < b_2 < 1 - \max(0, B_{21}) - \max(0, B_{22}) .$$

Note that under no conditions may the components of **b** lie outside the range zero to one.

During an inversion many different values of **P** are used in the forward model. Alternative optimization algorithms primarily differ in the way that they choose new values of **P**, so it is important to understand what effect making different changes to **P** has on the attractor. Figure 4 shows the attractors generated by a sequence of IFS's with $k = 3$. These are $f_1, f_2, \cdots, f_6$, where f_1 is the Sierpinski's gasket, and for frames $m = 2, 6$ every parameter of f_m differs from the corresponding parameter of f_{m-1} by a small increment:

$$\mathbf{P}_m = \mathbf{P}_{m-1} + \Delta\mathbf{P} . \tag{9}$$

The components of $\Delta\mathbf{P}$ are random numbers drawn from a uniform distribution, normalized so that the magnitude of $\Delta\mathbf{P}$, $|\Delta\mathbf{P}|$ (the square root of the sum of squared components of $\Delta\mathbf{P}$), equals 0.2. The continuous small change in **P** from frame to frame is manifested as a continuous gradual change in the attractors. A larger value of $|\Delta\mathbf{P}|$ would produce a more rapid variation in attractors.

The most general affine transforms that operate in two dimensions have four arbitrary entries in each $\mathbf{B}_i$ matrix, and two arbitrary values in each $\mathbf{b}_i$ vector, which makes **P** an $n = 6k$ dimensional vector for an IFS composed of k affine transforms. By holding some components of **P** fixed or limiting their variation we can produce attractors that have desired properties. As well as making the inversion procedure more efficient by reducing the extent of the parameter space to be searched, these constraints make the inversion more robust by conditioning it on known geological conditions. Formally, **P** is defined as the vector composed of all the parameters characterizing the IFS, but in practice we use **P** to denote only those parameters that can be varied during the inversion.

An IFS with $k = 2$ which has constant matrices of the form

$$\mathbf{B}_1 = \mathbf{B}_2 = \begin{bmatrix} 0.5 & 0.0 \\ 0.0 & 0.5 \end{bmatrix} = 0.5\,\mathbf{I} \tag{10}$$

and variable vectors $\mathbf{b}_1$ and $\mathbf{b}_2$ produces a vector $\mathbf{P}$ which has only four components. All the attractors produced by such an IFS are line segments, with endpoints determined by the values of $\mathbf{b}_1$ and $\mathbf{b}_2$. For the first frame of Figure 5a, $\mathbf{b}_1 = (0.0, 0.5)$ and $\mathbf{b}_2 = (0.5, 0.0)$; for the other frames, $\mathbf{b}_1$ and $\mathbf{b}_2$ are incremented by random numbers drawn from a uniform distribution. For Figure 5, in contrast to Figure 4, the original value of $\mathbf{P}$ and different value of $\Delta\mathbf{P}$ is used for each frame:

$$\mathbf{P}_m = \mathbf{P}_1 + \Delta\mathbf{P}_m \,. \tag{11}$$

For each frame of Figure 5a, the magnitude of the vector of random increments, $|\Delta\mathbf{P}_m|$, equals 0.6.

If both the $\mathbf{B}$'s and $\mathbf{b}$'s are allowed to vary, curvilinear attractors are formed, as shown in Figures 5b and 5c. For the small value of $|\Delta\mathbf{P}_m| = 0.2$ used in Figure 5b, all the attractors look similar to the original one. This would be a useful constraint if the attractor represented a region of enhanced permeability whose orientation was known *a priori*, such as a regional fracture set or buried stream channel. In Figure 5c, the variation in parameters is larger, $|\Delta\mathbf{P}_m| = 0.6$. Despite the large variability between the attractors, they all share the characteristic of being rather 'stringy', that is, they do not fill up the plane very well. This characteristic is quantified by a measure known as the fractal dimension. A straight line has a fractal dimension of one, whereas a curve that doubles back on itself so much that it covers the entire plane has a fractal dimension of two. Figures 5d and 5e show attractors created by IFS's with $k = 3$ and $k = 4$, and large variations in parameters ($|\Delta\mathbf{P}_m| = 0.6$). Although there is a large variability amongst the attractors, they tend to be more 'blocky' and less stringy as k increases, that is, fractal dimension tends to increase with k.

As an alternative to considering each $\mathbf{B}_i$ as composed of four independent entries, one can construct $\mathbf{B}_i$ as a rotation matrix

$$\mathbf{B}_i = C_i \begin{bmatrix} \cos\theta_i & -\sin\theta_i \\ \sin\theta_i & \cos\theta_i \end{bmatrix}, \tag{12}$$

where C_i is a contractivity factor ($0 < C_i < 1$) and θ_i is a rotation angle. This formulation reduces the dimension of $\mathbf{P}$ from six to four per affine transformation, but still allows a great variety of attractors, as illustrated in Appendix A.

FEATURES OF THE IFS INVERSION

Mapping the Attractor to a Hydrologic Property Distribution

To use the IFS attractors in a hydrologic inversion we need to prescribe how the attractor determines the spatial distribution of hydrologic properties in the mathematical model used to simulate the well test, which is called TRINET [*Karasaki*, 1987]. TRINET is a finite element model which calculates fluid flow in a lattice of one-dimensional finite elements (i.e., pipes) of porous or fractured medium. Although TRINET was originally developed to study fracture networks [*Long et al.*, 1991], it can also model porous media, as described in Appendix B. TRINET is well suited for use in a hydrologic inversion for several reasons:

- the one-dimensional finite element formulation is efficient computationally, enabling many forward calculations to be done,
- the lattice structure can be used effectively to represent highly channeled flow typical of strongly heterogeneous porous media,
- with the mapping from attractor points to hydrologic property distributions, described below, forward calculations for a tremendous variety of hydrologic settings can be done without changing the underlying lattice.

According to Equation (2) an attractor is formed by an infinite number of iterations, so it contains an infinite number of points. In practice we can only treat a finite number of points, so we take only a finite number of iterations I in Equation (2). If the starting set A_0 contains just one point, then the number of attractor points is $M_0 = k^I$. For typical applications $M_0 \approx 1000$ is large enough to resolve attractors adequately, implying that for $k = 4$, $I = 5$ is a sufficient number of iterations.

The attractor is defined on the unit square: $0 < x < 1$, $0 < y < 1$, and we need to choose a scale factor to map the unit square to the spatial domain where hydrologic-property variations affect the well-test response, that is, the region near the wells. We then superimpose the attractor on the TRINET lattice and modify the hydrologic properties (transmissivity T and storativity S) of the lattice elements adjacent to each attractor point, as illustrated in Figures 6 and 7.

The transmissivity and storativity that are unaffected by any attractor points are referred to as the base values T_0 and S_0. The effect of attractor points can be additive or multiplicative. If M attractor points are closest to a given lattice element, the additive algorithm gives

$$T = T_0 + M\Delta T \quad S = S_0 + M\Delta S \ , \tag{13}$$

and the multiplicative algorithm gives

$$T = T_0 \Delta T^M \quad S = S_0 \Delta S^M \ , \tag{14}$$

where ΔT and ΔS are the contribution for each attractor point. With the additive algorithm, choosing a positive value of ΔT or ΔS means that the attractor points increment T or S, whereas choosing a negative value means that attractor points decrement T or S. With the multiplicative algorithm, a value of ΔT or ΔS greater than one increments T or S, and a value less than one decrements T or S. The choice of additive or multiplicative algorithm and the sign and magnitude of ΔT and ΔS are arbitrary, but may be used to incorporate features of the geological setting in the mathematical model. For example, for a fractured rock T and S generally increase or decrease together, along with fracture aperture. In contrast, for a sand/clay aquifer system, increases in S are accompanied by decreases in T, as clay content increases. Furthermore, using the multiplicative algorithm for a parameter is equivalent to using the additive algorithm for the log of the parameter, making the additive algorithm for S and the multiplicative algorithm for T a natural choice for typical geologic media in which the variability of T is greater than the variability of S. Note that the value of M for each lattice element is proportional to M_0, the total number of points in the attractor. The value M_0 must be large enough to allow sufficient resolution of the attractor on the lattice, but it is preferable to give attractor points greater impact by increasing ΔT and ΔS rather than M_0 because the mapping of attractor points to lattice elements is computationally intensive.

For a variable-density lattice, the contribution of an attractor point to the overall hydrologic property distribution tends to be greater in coarse regions of the lattice than in fine regions. Thus, a given attractor will not produce the same hydrologic property distribution for two different lattices. This does not cause a problem in the inversion because only one lattice is used, but it means that a picture of the attractor provides only a qualitative representation of the hydrologic property distribution and a quantitative measure must come from the T or S distribution itself, such as is shown in Figure 7b.

An extension of the mapping algorithm has been developed in which some attractor points increment hydrologic properties, while other points decrement them, in contrast to the algorithms described by Equations (13) and (14) in which all attractor points act in the same manner. This approach, which we call the plus-minus algorithm, has the advantage that the base values T_0 and S_0 can represent average values of transmissivity and storativity, while the attractor points create fluctuations around the average. The plus-minus mapping algorithm is based on ideas from

Barnsley [1988, chap. 9] where a method for constructing a measure on an IFS attractor is given. First, each of the affine transforms which comprise the IFS is labeled either positive or negative. A point on the IFS attractor is then labeled positive or negative according to which affine transform was used last in its generation. If the attractor point is labeled positive, then Equation (13) or (14) is used as written to modify T and S; if it is labeled negative, then Equation (13) uses $-\Delta T$ and $-\Delta S$, and Equation (14) uses ΔT^{-1} and ΔS^{-1}. For an IFS composed of k affine transforms, the plus-minus algorithm tends to produce k discrete regions of high or low transmissivity and storativity. Several attractors produced by this procedure are illustrated in the application section of the paper.

An alternative approach for enabling both incremented and decremented hydrologic properties would be to use two completely independent attractors, one with points that increment properties and the other with points that decrement properties. Although this approach would double the number of parameters needed, it could greatly increase the applicability of the inversion method to different geological settings. A natural extension would be to use independent attractors to represent transmissivity and storativity distributions, if the geological model did not provide any information on the relation between these properties.

Construction of an Objective Function

The objective function, which quantifies the mismatch between the calculated and observed drawdowns for a given value of **P**, is called the energy E and is given by

$$E = \frac{N_0}{N}\sum_{1}^{N}(\ln h_c - \ln h_o)^2 , \tag{15}$$

where h_c and h_o are calculated and observed drawdowns, respectively, N is the number of observations available, and $N_0 = 100$ is a constant introduced to make the energy a convenient magnitude. Based on the physics of the flow problem, log drawdown is a more appropriate variable to include in E than drawdown itself. Mathematically, if we assume independent identically distributed Gaussian random errors in the $\ln h_o$ measurements, E is directly proportional to the log likelihood of the well response. Hence minimization of E corresponds to the statistical procedure of maximum likelihood estimation. See *Carrera and Neuman* [1986a and 1986b] for a discussion of these ideas and a more general formulation of E as a quadratic form based on the correlation structure of the measurement errors. The sum from 1 to N in Equation (15) runs over all observation wells (including the pumping well if drawdown is measured there) and all

observation times for a transient well test. For a steady-state well test, there is just one observation per well and all dependence on storativity drops out, leaving the transmissivity distribution as the only unknown to be determined by the inversion.

If the flow rate is held constant at the pumping well, the base values of transmissivity T_0 and storativity S_0 in the lattice can be inferred from the matching procedure, in much the same way as transmissivity and storativity for a uniform medium can be determined by matching drawdowns to a Theis type curve. In the calculation of the energy E, the drawdown curves calculated with trial values of T_0 and S_0 (and the contribution from the attractor) are shifted along the $\ln t$ axis by an amount Δ_1 and along the $\ln h$ axis by an amount Δ_2, with Δ_1 and Δ_2 chosen to minimize E. Then multiplying the trial value of T_0 by e^{Δ_2} yields the best-fit base transmissivity, and multiplying the trial value of T_0/S_0 by e^{Δ_1} yields the best-fit value of that ratio. Finally, multiplying the trial value of S_0 by $e^{\Delta_2-\Delta_1}$ yields the best-fit base value of storativity. For steady-state drawdowns arising from a constant-flow test, a shift of the $\ln h$ values may be used to determine T_0.

In typical analyses of transient well tests, the observed drawdowns that are included in the energy for each well are uniformly distributed in log time, but the form of Equation (15) makes it easy to account for a variety of special conditions. For example, if early-time drawdowns are thought to be controlled by well-bore effects or late-time drawdowns by distant boundaries not included in the model, they can simply be eliminated from the sum. If some observed data points are deemed more reliable than others due to differences in instrumentation, the energy can be weighted in their favor by including only a fraction of the less reliable points. Similarly, if certain responses are presumed to illustrate a key system feature, the inversion can be encouraged to find it by increasing the number of such observation points. Such weighting of different data points can also be accomplished formally with an energy function based on a quadratic form, as mentioned above.

In principle, the sum in Equation (15) could include drawdowns from multiple steady-state or transient well tests, a procedure we call co-inversion, but so far we have just analyzed single tests. Furthermore, for a well test in which the head is prescribed at the pumping well, the observed and calculated flow rates at the pumping well could also be included in the energy function. In this case, the prescribed head boundary condition eliminates the possibility of curve-shifting along the $\ln h$ axis to match observed data. Finally, the energy could include a comparison of model hydrologic properties and prior estimates of hydrologic properties, arising from,

for example, well tests not included in the inversion or from non-hydrologic work such as core measurements or geophysical surveys. The ability to tailor the objective function to include all available data is one of the strengths of the inverse method.

Optimization Algorithm

The term 'optimization algorithm' describes how new trial values of the n-dimensional vector $\mathbf{P}$ are chosen during the IFS inversion. Several optimization algorithms from standard numerical libraries have been used, and a more systematic study of their strengths and weaknesses is planned for future work, thus little emphasis is given to choices regarding their use in the applications presented in the following section. For all the optimization algorithms, the inversion is halted when the energy E drops below a specified value $E_{\min}$. Theoretically, the choice of $E_{\min}$ could be made to reflect the precision of drawdown measurements, but in practice oversimplification of the conceptual and numerical models usually contributes greatly to the discrepancy between modeled and observed drawdowns. Hence $E_{\min}$ is generally chosen rather heuristically, by requiring that the corresponding match between model and observed drawdowns is deemed "good enough."

The downhill simplex and direction set methods [*Press et al.*, 1986] both choose new values of $\mathbf{P}$ by interpolating or extrapolating toward lower values of E. In the downhill simplex method an $(n+1)$-dimensional 'amoeba' flows across the n-dimensional parameter space until it finds a minimum value of $E(\mathbf{P})$. In the direction set method a set of n orthogonal directions that span the n-dimensional parameter space is chosen randomly, then successive one-dimensional minimizations are done along each direction. For both these methods, computation time increases dramatically as the the number of unknown parameters n increases.

In contrast to the above methods, which make 'intelligent' choices for the values of $\mathbf{P}$ to try, simulated annealing [*Metropolis et al.*, 1953] tries new values of $\mathbf{P}$ randomly. The energy E' obtained using parameters $\mathbf{P}' = \mathbf{P} + \Delta\mathbf{P}$, where $\Delta\mathbf{P}$ is a random vector, is compared to the energy E obtained with the original $\mathbf{P}$. If $E' < E$, then $\mathbf{P}'$ replaces $\mathbf{P}$ as the current best set of parameters, another random $\Delta\mathbf{P}$ is chosen and the procedure is repeated. If $E' > E$, the $\mathbf{P}'$ might replace $\mathbf{P}$, with the probability of replacement given by

$$e^{(E-E')/\tau}, \tag{16}$$

where τ is a parameter known as the temperature, which determines how difficult it is to accept an increase in energy. Both $|\Delta\mathbf{P}|$ and τ start large and decrease during the course of the

inversion. Thus early in the inversion, highly varied attractors are tested and it is easy to get out of local minima of the energy function. Later, when E is smaller, subtle changes in attractors are tested, and minima are not escaped easily.

Simulated annealing seems to work well for hydrologic inversions, and it has an advantage over the previously described methods in that computation time does not directly increase with dimension n. However, as energy E decreases, more and more unaccepted values of **P** are tried, making the method inefficient. An approach known as simplex annealing [*Press and Teukolsky*, 1991] combines features of the downhill simplex and simulated annealing, in an effort to improve efficiency by making more intelligent choices for new values of **P** while at the same time including a random component to maintain the ability to jump out of local minima. This method appears very promising.

To ensure that an IFS converges to a finite attractor all of whose points lie within the unit square, the restrictions on the components of **P** given in Equations (7) and (8) are imposed. This is easily done when simulated annealing is used, by simply rejecting any trial $\mathbf{P}'$ that does not satisfy Equations (7) and (8) and using a different random $\Delta\mathbf{P}$ to create another trial $\mathbf{P}'$. This rejection algorithm cannot be so easily accommodated in the other optimization algorithms because trial values of **P** are chosen intelligently rather than randomly. Instead of rejecting a trial value of **P** entirely, the components of **P** violating Equations (7) or (8) are set to the bounding values. This approach has not been totally satisfactory, because the optimization algorithm tends to get stuck in corners of parameter space (especially for artificially simple synthetic problems). Further studies are planned to improve this procedure, because the addition of intelligence to the choices of **P** is a highly desirable feature.

APPLICATION OF THE METHOD

It is apparent from the previous section that to use the IFS inversion method one must specify a number of parameters that are not modified during the course of the inversion, but rather control the way in which the inversion operates. These parameters, known as control parameters, include such choices as the density and nesting of the lattice, the scale factor to map the attractor to the lattice, the number of affine transforms k, which components of the affine transforms may vary, the total number of attractor points M_0, and the size and type of property increments ΔT and ΔS. Choosing the control parameters provides an opportunity to condition the inversion on geological or other additional information, so that it will produce a model that is consistent with all known information about the system, as well as matching the hydrologic response. Additionally, one must specify the parameters that control the optimization algorithm, such as the temperature and increment schedules for simulated annealing; these choices affect the efficiency of the inversion.

INVERSION OF SYNTHETIC DATA

The only direct way to check if a hydrologic inverse method works is to generate synthetic well-test data from a known model and see if the inversion recovers the hydrologic property distribution of the model. It is desirable to start with simple synthetic data, to clearly illustrate what the inversion is doing, but it is necessary to also use realistic synthetic data (i.e., data including noise, models representing geologically realistic heterogeneities) to fully test an inversion method. The present studies are quite simple, and further work remains to be done.

Linear High-Transmissivity Feature

The first synthetic problem is a well test conducted in an aquifer with a single highly permeable linear feature, which might represent a buried stream channel or the trace of a conductive fault. The transmissivity of the linear feature is about 500 times greater than the background value and its storativity is unchanged from the background value. The transmissivity distribution and the lattice used for the calculations are shown in Figure 7b.

As described in the previous section, a linear heterogeneity can be described by an IFS with $k = 2$ of the form

$$f(A) = g_1(A) \cup g_2(A), \tag{17}$$

where

$$g_i(\mathbf{x}) = 0.5\,\mathbf{I}\,\mathbf{x} + \mathbf{b}_i\ . \tag{18}$$

This IFS has only four parameters, the two components of $\mathbf{b}_1$ and $\mathbf{b}_2$, which determine the length and orientation of the line segment. The linear feature shown in Figure 7b was created using an IFS with **P** given by Equation (18) and $\mathbf{b}_1 = (0.35,0.45)$ and $\mathbf{b}_2 = (0.19,0.19)$, a total of $M_0 = 1024$ attractor points, and the additive algorithm with $\Delta T = 10T_0$. The attractor itself is shown in Figure 7a. During the well test, a central well was pumped at a constant rate and transient drawdowns were calculated for four surrounding observation wells. The head was held constant at the outer boundary of the lattice. Well locations are marked by solid circles in Figure 7. Figure 8 shows the transient drawdowns calculated for this transmissivity distribution (the synthetic data), and the drawdowns that would occur for a uniform medium, for comparison. The effect of the high-transmissivity feature is clearly seen in the earlier, larger response of the upper well in Figure 8.

Because the synthetic hydrologic data was created using an IFS, it is straightforward to specify a very 'easy' problem for the IFS inversion: use the same values of the control parameters (T_0, S_0, ΔT, ΔS, M_0, k, n, etc.) as were used to create the data, then, if the inversion can find the correct values of **P**, the resulting model will be identical to that used to create the synthetic data, and E will be identically zero. Table 1 summarizes the results of six inversions done using simulated annealing with different random seeds. In all cases, the initial annealing temperature was $\tau = 3.6$, the initial increment in parameters was $|\Delta\mathbf{P}| = 0.6$, τ and $|\Delta\mathbf{P}|$ were decreased 1% each time a trial attractor was accepted, and the inversion was halted when $E \le E_{\min} = 3.6$. For comparison, the energy for a uniform medium with no attractor is $E = 46$ and the energy for the first attractor tried, a horizontal line segment through the center well, is $E = 860$. Figure 9 shows the energy variation over the course of the inversion for case 1E. The energy decline for accepted iterations is far from monotonic, reflecting the relatively large value of τ being used. Figure 8 shows the calculated drawdowns versus time for the final iteration of Case 1E, which yields an energy $E = 1.7$; the agreement with the synthetic data is very good, in effect justifying the choice of $E_{\min}$. The attractors found for the six cases are shown in Figure 10. Four of the six closely match the input attractor (Figure 7a), whereas 1A and 1F differ somewhat, illustrating the variability in transmissivity distribution that yields essentially the same well-test response.

The two attractors that least resemble the correct transmissivity distribution (1A and 1F) are in fact the two with the highest energy, suggesting that specifying a smaller value of $E_{\min}$ would yield a more unique attractor. While this is true in the present case, using an overly small a value

of E_{min} can be problematical. For real-world problems, in which the mathematical model is generally an extremely simplified representation of reality and well-test data contains noise, using a relatively large value of E_{min} ensures that effort spent during the inversion is used to match the main features of the drawdown curves, rather than small variations which may not reflect the overall hydrologic behavior of the system. For synthetic data, instrument noise and conceptual-model errors can be eliminated, but computer round-off error cannot, so even in this case an overly small value of E_{min} can be counterproductive. For example, an attractor given by $\mathbf{P} = (0.19,0.19), (0.35,0.45)$, which is mathematically identical to the correct attractor $\mathbf{P} = (0.35,0.45), (0.19,0.19)$, yields an energy $E = 1.1$, because a few attractor points located nearly midway between lattice elements are mapped to different elements. Hence, specifying a value of $E_{min} < 1.1$ would require that effort be spent during the inversion to reproduce round-off errors rather rather than hydrologic behavior.

For a less constrained inversion, we allow all entries of the affine transforms to vary, increasing the dimension of the parameter space from 4 to 12. As shown in Figures 5b and c, the trial attractors are no longer constrained to be line segments. As before, six inversions were done using simulated annealing with $E_{min} = 3.6$, using different random seeds. The range of computer times used was about the same as before; the final attractors are shown in Figure 11. In contrast to the previous case (Figure 10), there is now significant variability among the attractors. All the attractors succeed in identifying a high-transmissivity channel between the middle and upper wells, but most show fictitious high-transmissivity channels elsewhere as well. A careful examination of Figure 11 indicates that none of the spurious high-transmissivity channels are located along pathways connecting the pumping well and the observation wells. The model can include these spurious high-transmissivity channels and still yield a low energy because the observation-well drawdowns are not very sensitive to these regions of the model. This insensitivity is a common problem when analyzing well tests involving a single pumping well and a limited number of observation wells, and doing multiple inversions is a powerful technique for identifying regions for which the well test provides no information. Rather than indicating a failure of the inversion method, non-uniqueness illustrates the limited nature of the information contained in the well-test response.

If we visually filter out those features not common to all the attractors in Figure 11, we begin to obtain a reasonable representation of the actual high-transmissivity feature. This visual filtering operation can be formalized by looking at the mean transmissivity distribution. Figure 12 shows the transmissivity distributions for each of the six inversions, corresponding to the

attractors shown in Figure 11. Figure 13 shows the mean transmissivity distribution, formed by calculating the transmissivity of each lattice element as the mean over the six inversions. The mean transmissivity distribution compares favorably with the actual distribution (Figure 7b), although the spurious high-transmissivity channels are still apparent. If the spurious channels represent random errors, averaging over more inversions should minimize their effect. The average transmissivity distribution for 30 inversions, also shown in Figure 13, better replicates the synthetic data, supporting this hypothesis.

A more basic way to eliminate spurious attractor points is to analyze well-test data that is sensitive to larger areas of the aquifer, which can be accomplished by using more observation wells, since Figure 11 indicates that the response at an observation well is most sensitive to the region directly between the pumping well and observation well. Unfortunately, drilling many wells may be economically or physically impossible. An alternative approach is to do a series of flow tests using different wells as the pumping well, as shown schematically in Figure 14, then combining all the drawdown responses in the energy.

Square Zone of Contrasting Transmissivity and Storativity

The second synthetic problem considers an aquifer with a central square region whose transmissivity and storativity are either 100 times greater ('high anomaly') or 100 times less ('low anomaly') than the values of the surrounding area. Six wells surround the anomaly, as shown in Figure 15. One well is pumped and transient drawdowns are measured in the other five. Head is held fixed at the outer boundary of the lattice. Figure 16 shows the transient drawdowns at the observation well locations for the high and low anomalies, and for a uniform medium. Compared to the uniform medium response, the high anomaly strongly affects the drawdown curves at all observation wells, whereas the low anomaly primarily affects the wells across the anomaly from the pumping well.

Table 2 summarizes the results of three inversions with $k = 3$ done for the high anomaly, using simulated annealing with different random seeds. In each case, the additive algorithm was used with $\Delta T = 10T_0$ and $\Delta S = 10S_0$, and $E_{\min} = 1.6$. The energy for a uniform medium with no attractor is $E = 92$, the energy for the first attractor tried, the Sierpinski Gasket shown in Figure 17, is $E = 85$. The drawdowns for Case 2A are shown in Figure 18; the agreement with the synthetic data is very good. The attractors for each case, shown in Figure 19, all succeed in concentrating points within the anomaly.

Three inversions with $k = 3$ were also done for the high anomaly using attractors that decrement transmissivity and storativity. For decremented transmissivity and storativity, an ideal attractor would have points uniformly distributed around the outside of the anomaly. Although the energies for these inversions ($E = 47$ to 58) are only about a factor of two lower than the energy for a uniform medium, the attractors, shown in Figure 20, all succeed in concentrating points outside the anomaly.

By construction, an attractor is anchored to the k points found by iterated application of each of the k affine transforms that make up the IFS (e.g., the lower left corner point of the Sierpinski Gasket shown in Figure 17 results from repeated application of $g = 0.5\mathbf{I} + (0,0)$ the upper right corner from $g = 0.5\mathbf{I} + (0.5,0.5)$, and the upper left corner from $g = 0.5\mathbf{I} + (0,0.5)$). This k-fold anchoring is consistent with the increase in attractor fractal dimension with k observed in Figure 5, and implies that the attractors tend to contain k-fold features. Generally, higher values of k should be used to mimic more complicated structures. In particular, it is natural to try to outline a square anomaly using an IFS with $k = 4$. The attractors for two such inversions using the multiplicative algorithm with $\Delta T = \Delta S = 0.5$ are shown in Figure 21. Despite the appealing shape of the attractors, the energies are still rather high ($E = 38$ for both cases) reflecting only a qualitative match to the drawdowns, as shown in Figure 22.

Several inversions using the plus-minus algorithm were also done for the high anomaly, using an IFS with $k = 4$. Not surprisingly, the returned energies ($E = 6$–20) were better than for the decrement-only inversions, but worse than for the increment-only inversions. The attractors tend to concentrate the incrementing points within the anomaly, while putting the decrementing points outside it, as is illustrated in Figure 23.

Table 3 summarizes the results of three inversions with $k = 3$ for the low anomaly, with attractor points that decrement properties. The multiplicative algorithm was used, with $\Delta T = \Delta S = 0.5$. Although the energies ($E = 4$–8) are not as low as for the high-anomaly inversions with incremented properties (Table 2), the drawdowns, shown in Figure 24 for Case 2L, reproduce the main features of the synthetic data reasonably well. Because the energies never reached the specified value of $E_{\min} = 1.6$, an alternate stopping criterion was used, in which an inversion was halted when E did not decrease after many (usually several thousand) iterations. The attractors, shown in Figure 25, all succeed in concentrating the points within the anomaly.

In order to investigate the sensitivity of the inversion process to well location, inversions with $k = 3$ were done considering wells located inside and outside the anomaly, in both regular

and irregular patterns, as shown in Figure 26. Table 4 summarizes the results of the inversions and indicates that in all cases the IFS inversion method matches the hydrologic response. The high-anomaly inversions use an attractor which increments properties using the additive algorithm and $\Delta T = 10T_0$ and $\Delta S = 10S_0$. The low-anomaly inversions use an attractor which decrements properties using the multiplicative algorithm and $\Delta T = \Delta S = 0.5$. The attractors (not shown) successfully concentrate points within the anomaly. Intuitively, one would expect that if an anomaly produces a small signal in the drawdown curves (for example, because it has similar properties to the surrounding area, or is of very small or very large spatial extent compared to the dimensions of the well field), the IFS inversion method would have less success identifying it. Studies to quantify this notion are underway.

INVERSION OF REAL DATA FOR A POROUS MEDIUM – KESTERSON RESERVOIR

A variety of well tests have been conducted on a shallow aquifer system composed of interbedded sands, silts, and clays at Kesterson Reservoir, located in the San Joaquin Valley in central California [*Yates*, 1988]. The hydrologic properties of the aquifer/aquitard system are needed in order to study the transport of various forms of selenium and other salts between surface waters and underlying aquifers. The aquifer studied in the present example is about 18 m thick, and is underlain by an impermeable clay layer and overlain by a leaky aquitard. A multi-well transient test was analyzed to infer the spatial distribution of transmissivity in the aquifer. Both steady-state and transient single-well tests and multi-well pulse tests have also been conducted at the site.

In the test under consideration, a central well was pumped at a constant rate of 6×10^{-3} m^3/s and transient drawdowns were measured at eight observation wells located 15 to 107 m away from the pumping well. All the wells were screened over the middle third of the aquifer thickness. The test lasted 5 hours, with the first observations made about 5 seconds after pumping commenced.

Quasi-three-dimensional Analysis

Initial studies used the two-dimensional nested lattice shown in Figure 27 to represent the aquifer. The well-field is shown by the solid circles, with the pumping well at the center ($x = 0$, $y = 0$). The nested lattice design is practical for modeling flow in porous media, where fine resolution is needed to represent flow near wells adequately, but the lattice must extend far beyond the well field to realistically implement pressure boundary conditions. Fine resolution is undesirable beyond the well field, because it greatly increases the size of the calculation without

improving the ability of the model to predict flow or pressure at the well field. At the outer boundary of the lattice the head was held constant, with the extent of the lattice chosen so that the cone of depression would not reach the boundary during the duration of the well test.

Use of a two-dimensional lattice requires that the wells be modeled as fully penetrating and that the upper and lower confining layers be considered impermeable. The late-time slopes of the drawdown versus time curves calculated by this model were consistently steeper than observed slopes. Because geological information and other hydrologic inversion studies [*Yates*, 1988] suggested that leakage occurred through the upper confining layer, it was decided to use a quasi-three-dimensional model in which leakage from an overlying aquitard could be included in an approximate way, as described in Appendix B, which required the addition of approximately 700 nodes and elements to the lattice shown in Figure 27. The ratio of the aquitard vertical permeability to the base value of the aquifer horizontal permeability was estimated to be 10^{-3} by matching the slopes of the late-time portion of the drawdown curves to observed values. The specific storage of the aquitard was assumed to correspond to the base value of storativity of the aquifer. These parameters did not vary during the inversion (i.e., they were unaffected by the location of attractor points). Vertical flow within the aquifer itself was not included in this model, so partial penetration effects were not accounted for.

Figure 28 shows the observed drawdown versus time curves and those calculated assuming a medium with uniform transmissivity and storativity (no attractor). The energy of the uniform-medium solution is $E = 25$. Note from Figure 27a that the observation wells are divided into two groups: four 'inner' wells are located between 14 and 16 m away from the pumping well, and four 'outer' wells are located between 60 and 107 m away. Figure 28 shows that the worst match between the uniform medium calculation and the observed data is for the outer well on the left, and among the inner wells the worst match is again found for the well on the left. These qualitative observations suggest that the attractor might show some special characteristics on the left side.

The attractor was scaled to lie in the region of the lattice given by $-150 < x < +150$ m and $-150 < y < +150$ m. Geological information and previous well-test analysis [*Yates*, 1988] indicate that storativity is far less variable than transmissivity in the Kesterson setting, so attractor points represent changes in transmissivity only. Table 5 summarizes the results of three inversions with $k = 4$ with decremented transmissivity. The multiplicative algorithm was used, with $\Delta T = 0.5$. Case K1 used simplex annealing with $n = 12$ parameters (the rotation form of the **B**

matrix given by Equation (12), with only θ's and **b**'s variable) for most of the inversion. The inversion stopped at $E = 1.7$ and was restarted with all parameters variable ($n = 16$). Cases K2 and K3 used simulated annealing with $n = 12$ and $n = 16$, respectively. The drawdowns calculated for Case K3 are shown in Figure 28, the agreement with the observed drawdowns is very good.

Figure 29 illustrates the attractors for Cases K1, K2, and K3. Although they by no means produce a unique picture of the transmissivity distribution, they do show a number of features in common. The attractors are all relatively compact structures overlying the inner observation wells. In each case there is a point-free region between the pumping well and the inner left observation well, providing a high-permeability path between them, which accounts for the large, early response of that observation well. Additionally, each case shows a strong concentration of points between the inner and outer wells on the left side, which accounts for the small, late response of the outer left observation well.

Because of the nested nature of the lattice used for the calculations the attractors themselves provide only a qualitative picture of the transmissivity distributions. Two quantitative representations are shown in Figure 29. The first displays the central portion of the lattice with the thickness of each element proportional to the transmissivity of that element. This is a straightforward representation of the transmissivity distribution used for the flow calculation, but the increase in element transmissivity that occurs as the lattice gets coarser tends to overshadow the variations in transmissivity caused by the attractor points, making the pictures cumbersome to interpret. The final display in Figure 29 attempts to alleviate this problem, by eliminating the lattice from the picture and plotting the effective transmissivity of the aquifer that the lattice represents. For each element in the lattice, transmissivity T is divided by element length L to give effective transmissivity $\tilde{T}$, as described in Appendix B. Then a square centered on the element is filled with a dot pattern whose density is proportional to $\tilde{T}$.

It turns out that for the mapping algorithm used, attractor points have a greater effect on transmissivity in the coarser regions of the lattice than in the finer central region around the inner wells. Thus each attractor yields a transmissivity distribution with an annular low transmissivity region between the inner and outer observation wells. Some inversions using incremented transmissivity were also done. These yielded higher energies than the decremented-transmissivity inversions for comparable numbers of forward calculations, suggesting that a geological model consisting of local low-permeability features (e.g., clay lenses) embedded in a

high-permeability background may be more appropriate than local high-permeability features (e.g., gravel bars) embedded in a low-permeability background. Figure 30 shows the three attractors that yielded the lowest energies ($E \approx 9$) of the incremented-transmissivity inversions. For the most part, attractor point locations are complementary to those for the decremented-transmissivity inversions, yielding a consistent picture of the aquifer transmissivity distribution, with a low-permeability region just beyond the inner observation wells, and a high-permeability region further away.

Comparison with Previous Analysis

Yates [1988] used a two-dimensional axisymmetric porous medium model to analyze the interference test considered here. Her model differed from the present one by accounting for well partial penetration, allowing vertical variations in permeability in the aquifer, and requiring horizontal permeability variations to be radially symmetric and centered at the pumping well. She did not use a formal optimization algorithm, but ran repeated forward simulations of the interference test with different permeability distributions chosen by hand, using results of a series of single-well tests to guide the choices. Her best match to the observed drawdown curves is comparable to that shown in Figure 28, and was obtained using a composite aquifer model with a high-permeability zone in the vicinity of the inner wells, with a permeability about ten times that of the rest of the aquifer. Our results are consistent with this model in the vicinity of the inner wells. Yates used a ratio of aquitard vertical permeability to inner-zone-aquifer horizontal permeability of about 2×10^{-3}, twice as large as that used for the present study. The additional leakage provided by the higher permeability of the aquitard may eliminate the need for the high-permeability outer zone found in the present study.

Possible Further Studies

The Kesterson Reservoir site provides several opportunities for further development and testing of the IFS inversion method. To rigorously analyze the present interference test, we should use a fully three-dimensional model in which the transmissivities of both the aquifer and leaky aquitard vary. The IFS inversion method could be applied to three-dimensional problems with only minor modifications, but the computational effort of an inversion would be greatly increased. Not only will the forward calculations require far more computational time due to a larger lattice, but a three-dimensional attractor has 12 parameters for each affine transformation, compared to 6 for a two-dimensional attractor, doubling the dimension of the parameter space

that must be searched by the inversion. One possibility would be to use a three-dimensional lattice to properly account for vertical flows arising from well partial penetration, but to limit the attractor and corresponding transmissivity variations to two-dimensional structures within the aquifer to minimize the number of parameters. Before embarking on three-dimensional inversions we need to streamline all aspects of the inversion code.

It would be very interesting to condition the inversion of the interference test by the results of the single-well tests, as was done by *Yates* [1988]. Such conditioning could be done in a straightforward way by co-inverting all the available well tests, however, this would be computationally intensive as each forward calculation would have to include the interference test and all the single-well tests. A more efficient approach might be to simulate just the interference test but to add a penalty term to the objective function if the transmissivity in the neighborhood of a well contradicted the value inferred from that wells individual well test.

One of the appealing features of a fractal model for a hydrologic property distribution is its ability to scale up the model from a relatively small-scale well test to a large-scale regional model, which arises naturally from the self-similar nature of fractals. A second interference test was done at Kesterson, studying the same aquifer/aquitard system at a nearby well field. It could be worthwhile to invert this second test independently of the present work, and then co-invert them both, using a larger lattice encompassing both well fields, to determine whether a fractal model of the transmissivity distribution is appropriate at this larger scale.

INVERSION OF REAL DATA FOR A FRACTURED MEDIUM – STRIPA

At the Stripa mine in Sweden, we have been investigating the hydrology of a subvertical fracture zone called the H-zone within a 150 m × 100 m × 50 m block of rock. A series of seven boreholes (C1, C2, C3, C4, C5, W1, W2) penetrate this zone. Each of these boreholes was fitted with packers that isolate a test interval in the H-zone. An interference test, called the C1-2 test, was conducted in these holes. In this test, the C1 hole was pumped at a constant rate from a packed-off interval in the H-zone. Responses were measured in the other holes in intervals packed-off in the H-zone. A second experiment, called the Simulated Drift Experiment (SDE), measured the steady-state flow rate from the H-zone into six parallel holes drilled within a 1 m radius (the D-holes), which were held at a constant drawdown. The entire data set is described in *Olsson et al.* [1989] and *Black et al.* [1991]. An inversion of this data using simulated annealing is given in *Long et al.* [1991].

Here we present results of three IFS inversions based on the C1-2 interference test. The models produced by the inversions were subsequently used to predict the flow rate into the D-holes in the SDE. We treat the H-zone as a two-dimensional feature, so the C-, D-, and W-boreholes appear as points where they penetrate the plane of the H-zone. A two-dimensional variable-density lattice, shown in Figure 31, was used to model the H-zone, in order to maximize detail in the vicinity of the D-holes, provide a large enough lattice to prevent the transients from reaching the boundary too soon, and minimize the number of elements and bandwidth. The finest lattice spacing is 1.5 m and the lattice extends 400 m from the center of the well field. The outer boundary conditions in the model were chosen to represent the estimated equilibrium head values.

C1-2 Interference Test

Figure 32 shows the observed drawdown versus time curves and those calculated assuming the H-zone has uniform transmissivity and storativity (no attractor). Three general features indicate the need for a heterogeneous description of the H-zone: The predicted drawdown at borehole W2 is much too large, the predicted drawdowns at boreholes C4, C2, and C5 are too small, and the predicted drawdowns at boreholes W1 and C3 are too big at early times but about right at later times. The drawdowns calculated using a uniform-medium model correspond to an energy of $E = 51$.

All three C1-2 inversions used IFS's with $k = 4$ in which all 24 parameters varied independently and the multiplicative mapping algorithm. For Case S1, in which the lowest energy was $E = 10$, the attractor points either incremented or decremented the transmissivity and storativity using the plus-minus algorithm, in Case S2 ($E = 9$) the attractor points incremented the transmissivity and storativity, and Case S3 ($E = 19$) the attractor points decremented transmissivity and storativity. The results of the three inversions are summarized in Table 6. Each inversion was halted after E had not decreased for many iterations. Figure 32 shows the drawdown curves and Figure 33 shows the energy variation over the course of the inversion for Case S1. Results for Cases S2 and S3 (not shown) are similar. Figure 34 shows the attractor which yields the lowest energy for each case and the corresponding hydrologic property distribution. The background values of transmissivity and storativity for the three inversions differ, because although each inversion started with the same value of T_0 and S_0, the amount the drawdown curves were shifted to yield the minimum energy, Δ_1 and Δ_2, differed from case to case. The middle and lower rows of Figure 34 show the transmissivity distributions with the different shifts taken into account by

plotting Te^{Δ_2}. These plots also represent the spatial variability of storativity, but not its absolute value, which would require plotting $Se^{\Delta_2-\Delta_1}$.

Figure 34 shows that each inversion creates a hydrologic property distribution in which transmissivity and storativity are larger in the region of the H-zone around boreholes C1, W1, C3, and C4 than elsewhere. This results in an improvement in all the predicted drawdown curves: the drawdown at borehole W2 is decreased by isolating W2 in a low-permeability region; the drawdowns at boreholes C2, C4, and C5 are increased because of the high-permeability region between boreholes C1 and C4; and for Cases S1 and S2 the response at boreholes W1, C3, and C4 is delayed by increasing storativity in their vicinity, whereas for Case S3 the response is delayed by an isolated low-permeability streak. The overall consistency between the hydrologic property distributions created by inversions in which attractor points have sharply contrasting effects is encouraging.

SDE Flow Rate Prediction

To use the models developed by inverting the C1-2 data to predict the flow rate into the D-holes during the SDE, we first shut in well C1 and allowed a steady-state head distribution to develop in each model. A drawdown of 220 m was then applied at the D-holes, and the steady-state flow rate into the D-holes was calculated. The calculated SDE flow rates range from 0.13×10^{-6} m^3/s for Case S2 to 0.22×10^{-6} m^3/s for Case S1 to to 0.38×10^{-6} m^3/s /min for Case S3, whereas the actual flow rate to the D-holes from the H-zone during the SDE was estimated to be about 0.2×10^{-6} m^3/s. The models created by the inversions with the lowest energies (Cases S1 and S3) best matched the SDE flow rate, whereas the model created by Case S3, with about double the energy, did no better than a uniform-medium model. Overall, we consider the performance of the IFS inversion on the Stripa data successful.

SUMMARY AND CONCLUSIONS

We have developed an inverse method to estimate hydrologic properties based on the analysis of hydrologic well tests. The trial hydrologic property distributions considered during the inversion process are generated using iterated function systems (IFS's), and are constructed to have self-similar or fractal geometry. Fewer parameters are needed to describe a self-similar geometry than a general heterogeneous geometry, improving the efficiency and robustness of the inversion. Equally important is that the final parameter set produces a hydrologic property distribution with a hierarchical structure, as is often seen in natural geological media. Constraining the parameters of the IFS during the inversion constrains the resulting attractor shapes, which may make it possible to limit the search for hydrologic property distributions to those consistent with conceptual geological models or with other additional information.

Application of a two-dimensional version of the IFS inversion method to idealized synthetic data and to field data from a sand/clay sedimentary sequence and a fractured granite has shown its promise, but further work remains to be done. We are investigating alternate methods for mapping the attractor to the lattice, in order to better represent geological structure. Another major task being undertaken is to analyze and improve the optimization algorithm. Optimization algorithms such as simplex annealing, which combine intelligent choices for new parameter values with the ability to escape local minima seem very promising. Finally, we are working to make the numerical simulation of the forward problem as efficient as possible. With the above improvements more computationally intensive problems can be tackled, such as using three-dimensional numerical models and co-inverting sequences of well tests.

The IFS inversion method does not always return a uniquely determined hydrologic property distribution. This is not a failure of the method itself, but rather reflects on the limitations of the information contained in the well-test response. By making multiple inversions of a given well test, and comparing the returned hydrologic property distributions, one can discern from the common features those regions which have the greatest influence on the well test and their hydrologic properties, and from the contradictory features those regions to which the well-test response is not sensitive.

As illustrated in Figure 14, co-inverting multiple well tests can make the analysis sensitive to greater portions of the flow region. This concept can be extended by co-inverting different kinds of data, for example adding seismic or electromagnetic measurements to the objective function, and adding the corresponding simulations to the forward calculation. A more economical

means of improving uniqueness is to condition the inversion of a hydrologic interference test by adding penalty terms to the objective function to reflect mismatches to known hydrologic property data. Another possibility would be to do a geostatistical analysis of each trial hydrologic property distribution and reject those which contradict observed geostatistical parameters.

One of the strengths of the hydrologic inversion method is that we use fluid flow to develop models that will be used to predict fluid flow. Predicting fluid flow is the ultimate goal for applications such as estimating water supply or optimizing oil recovery. For studies involving remediation of contaminated aquifers or storage of nuclear waste, understanding solute transport via fluid flow is the ultimate goal, rather than studying the flow itself, making the inversion of solute transport data desirable. Such inversion can be incorporated in the IFS framework in a straightforward manner, and may yield noteworthy results because the equation governing solute transport contains an advective as well diffusive term, which may strongly impact the inversion process.

APPENDIX A: CONSTRUCTING B AS A ROTATION MATRIX

As an alternative to considering each $\mathbf{B}_i$ as composed of four independent entries, one can construct $\mathbf{B}_i$ as a rotation matrix

$$\mathbf{B}_i = C_i \begin{bmatrix} \cos\theta_i & -\sin\theta_i \\ \sin\theta_i & \cos\theta_i \end{bmatrix}, \tag{A.1}$$

where C_i is a contractivity factor ($0 < C_i < 1$) and θ_i is a rotation angle. This formulation reduces the dimension of **P** from six to four per affine transformation but still allows a great variety of attractors, as illustrated in Figure A.1, frame (a). By holding some components of **P** constant, the effect of C, θ, and **b** can be demonstrated, as shown in frames (b) through (d). By allowing changes in θ and **b** while holding C fixed, a wide variety of attractor shapes can be created (frame (e)), with a further reduction in the dimension of **P** from four to three per affine transform.

APPENDIX B: THE NUMERICAL MODEL TRINET

Basic Formulation

The finite element model TRINET [*Karasaki*, 1987] calculates fluid flow and solute transport on a lattice of one-dimensional finite elements (i.e., pipes) of porous medium. TRINET incorporates an adaptive gridding algorithm to minimize numerical dispersion for transport calculations, but in the present application we use a fixed grid and calculate fluid flow only. The flow equation between the two nodes at either end of a one-dimensional finite element may be written as

$$S\frac{\partial h}{\partial t} = T\frac{\partial^2 h}{\partial x^2}, \tag{B.1}$$

where h is hydraulic head and S and T are the storativity and transmissivity, respectively, of the element. The lattice of elements need not be uniformly spaced; it can be two- or three-dimensional, and rectangular, triangular, or a combination thereof.

Representation of a Two-dimensional Porous Medium (a Confined Aquifer)

When applying the IFS inversion method to a porous medium, TRINET is used with a two-dimensional rectangular lattice to represent an areal view of an aquifer. It can be shown

[*Doughty*, 1993] that for lattice elements with transmissivity T, storativity S, a cross-sectional area of one, and length L, the effective aquifer transmissivity $\tilde{T}$ and storativity $\tilde{S}$ are given by

$$\tilde{T} = \frac{T}{L} \qquad \tilde{S} = \frac{2S}{L} . \tag{B.2}$$

As is customary in the hydrologic literature, the transmissivity $\tilde{T}$ is the product of aquifer hydraulic conductivity K and aquifer thickness, the storativity $\tilde{S}$ is the product of aquifer specific storage S_s and aquifer thickness, and hydraulic conductivity is intrinsic permeability divided by fluid viscosity.

For a lattice with variable spacing to behave as a uniform porous medium, element properties must vary with lattice spacing. A convenient variable lattice is a nested lattice in which a central fine region with spacing L is surrounded by a region with spacing aL, which in turn is surrounded by a region with spacing a^2L, and so on, so that the jth nested region has lattice spacing a^jL. Figure 27 illustrates such a lattice. One consistent prescription for lattice element properties is to require that as lattice spacing increases from L to a^jL, the element properties are modified as follows:

$$T \rightarrow a^jT \qquad S \rightarrow a^jS . \tag{B.3}$$

The ability of TRINET to properly model flow through a porous medium has been verified by comparing its results to the Theis solution [*Theis*, 1935] for transient radial flow in a confined homogeneous isotropic aquifer, in which a fully-penetrating well is pumped at a constant flow rate [*Doughty*, 1993].

Representation of a Quasi Three-dimensional Porous Medium (a Leaky Aquifer)

The two-dimensional aquifer model described in the previous section has completely impermeable confining layers above and below it. It is straightforward to extend the model to include small vertical flows into the aquifer through a leaky confining layer, which is presumed to remain at constant head. One new vertical element and one new constant-head node are added for each node in the original two-dimensional lattice. Each new element has storativity S', transmissivity T', length L', and a cross-sectional area of one. It can be shown that for a lattice spacing L, the effective confining layer vertical hydraulic conductivity $\tilde{K}'$ and specific storage $\tilde{S}_s'$ are given by

$$\tilde{K}' = \frac{T'}{L^2} \qquad \tilde{S}_s' = \frac{S'}{L^2} . \tag{B.4}$$

To account for the variable lattice density in a nested lattice, when the lattice spacing increases from L to $a^j L$, the TRINET properties are modified as follows:

$$T' \rightarrow a^{2j} T' \qquad S' \rightarrow a^{2j} S' . \tag{B.5}$$

The quasi-three-dimensional nested lattice has been verified by comparing TRINET results to an analytical solution [*Hantush and Jacob*, 1955] for transient radial flow in a homogeneous isotropic aquifer with a slightly leaky confining layer, in which a fully-penetrating well is pumped at a constant flow rate [*Doughty*, 1993].

NOTATION

A	set of points **x**
a	coarsening factor for a nested lattice
$\mathbf{B}$	matrix of affine transform
$\mathbf{b}$	vector of affine transform
C	rotation-matrix contractivity factor (Equation (12))
E	energy, the value of the objective function to be minimized by inversion
$E_{\min}$	stopping criterion for the inversion
f	iterated function system (IFS)
g	affine transform
h	head or drawdown (m)
I	number of iterations used to generate attractor
$\mathbf{I}$	identity matrix
j	level of nesting for a nested lattice
K	hydraulic conductivity (m/s)
k	the number of affine transforms in an IFS
L	lattice spacing, for a nested lattice the lattice spacing is $a^j L$ at the jth level of nesting (m)
M	number of attractor points affecting a lattice element
M_0	total number of attractor points
N	number of observed drawdowns included in the objective function
N_0	a constant to keep E a convenient magnitude (currently $N_0 = 100$)
n	dimension of parameter space
$\mathbf{P}$	vector of unknown parameters (entries of $\mathbf{B}$'s and $\mathbf{b}$'s)
$\Delta\mathbf{P}$	vector of random increments
$\lvert\Delta\mathbf{P}\rvert$	magnitude of vector $\Delta\mathbf{P}$ (square root of sum of squares of components of $\Delta\mathbf{P}$)
S	storativity
ΔS	contribution of attractor point to storativity
S_s	specific storage (m^{-1})
T	transmissivity (m^2/s)
ΔT	contribution of attractor point to transmissivity
t	time (s)
τ	temperature in simulated annealing algorithm
$\mathbf{x}$	coordinates of point (m)
x	distance (m)
y	distance (m)
Δ_1, Δ_2	amount of curve shift along the $\ln t$ or $\ln h$ axis, respectively, to minimize E
θ	rotation-matrix angle (Equation (12))

Subscripts and modifiers

c	calculated
o	observed
0	base value (unaffected by attractor points) or initial value
$'$	leaky confining layer property or trial value
$\bar{}$	effective porous medium property

Acknowledgements. The careful reviews of Akhil Datta Gupta of Lawrence Berkeley Laboratory and John Rice of the University of California, Berkeley are gratefully appreciated. This work was primarily supported by the Director, Office of Energy Research, Office of Health and Environmental Research, Subsurface Science Program, of the U.S. Department of Energy under Contract No. DE-AC03-76SF00098. The application to fractured media is based apon work supported by the National Science Foundation under Grant No. DMS-920054.

REFERENCES

Barnsley, M., *Fractals Everywhere*, Academic Press, Boston, 1988.

Black, J.H., Olsson, O., Gale, J.E., Holmes, D.C., Site characterization and validation, Stage 4, Preliminary assessment and detail predictions, Report TR 91-08, Swedish Nuclear Fuel and Waste Management Co., Stockholm, Sweden, 1991.

Carrera, J. and Neuman, S.P., Estimation of aquifer parameters under transient and steady state conditions: 1. Maximum likelihood method incorporating prior information, *Water Resour. Res.*, *22*(2), 199-210, 1986a.

Carrera, J. and Neuman, S.P., Estimation of aquifer parameters under transient and steady state conditions: 2. Uniqueness, stability, and solution algorithms, *Water Resour. Res.*, *22*(2), 211-227, 1986b.

Carrera, J. and Neuman, S.P., Estimation of aquifer parameters under transient and steady state conditions: 3. Application to synthetic and field data, *Water Resour. Res.*, *22*(2), 228-242, 1986c.

Doughty, C., Estimation of hydrologic properties of heterogeneous geologic media: An inverse method based on iterated function systems, Ph.D. Dissertation, Dept. of Material Science and Mineral Engineering, University of California, Berkeley, in preparation, 1993.

Hantush, M.S. and Jacob, C.E., Non-steady radial flow in an infinite leaky aquifer, *Trans., Amer. Geophys. Union*, *36*(1), 95-100, 1955.

Karasaki, K, A new advection-dispersion code for calculating transport in fracture networks, Earth Sciences Division 1986 Annual Report, LBL-22090, Lawrence Berkeley Laboratory, Berkeley, California, pp. 55-58, 1987.

Kitanidis, P.K. and Vomvoris, E.G., A geostatistical approach to the inverse problem in groundwater modeling (steady state) and one-dimensional simulations, *Water Resour. Res.*, *19*(3), 677-690, 1983.

Koltermann, C.E and Gorelick, S.M., Paleoclimatic signature in terrestrial flood deposits,

Science, 256, 1775-1782, 1992.

Long, J.C.S., Mauldon, A.D., Nelson, K., Martel, S., Fuller, P. and Karasaki, K, Prediction of flow and drawdown for the site characterization and validation site in the Stripa mine, Report No. LBL-31761, Lawrence Berkeley Laboratory, Berkeley, California, 1991.

Long, J.C.S., Doughty, C., Hestir, K., and Martel, S., Modeling heterogeneous and fractured reservoirs with inverse methods based on iterated function systems, in *Reservoir Characterization III*, Bill Linville, Ed., pp. 471-503, PennWell Books, Tulsa, Oklahoma, 1993.

Metropolis, N., Rosenbluth, A., Rosenbluth, M., Teller, A., and Teller, E., *J. Chem. Phys., 21*, 1087, 1953.

Olsson, O., Black, J.H., Gale, J.E. and Holmes, D.C., Site Characterization and Validation, Stage 2, Preliminary Predictions, Report TR 89-03, Swedish Nuclear Fuel and Waste Management Co., Stockholm, Sweden, 1989.

Press, W.H. and Teukolsky, S.A., Simulated annealing optimization over continuous spaces, *Computers in Physics*, Jul/Aug, 1991.

Press, W.H., Flannery, B.P., Teukolsky, S.A., and Vetterling, W.T., *Numerical Recipes: The art of scientific computing*, Ch. 10, Cambridge University Press, New York, 1986.

Theis, C.V., The relation between the lowering of the piezometric surface and the rate and duration of discharge of a well using ground-water storage, *Trans., Amer. Geophys. Union, 16*, 519-524, 1935.

Webb, E.K., Simulating the spatial heterogeneity of sedimentological and hydrogeological characteristics for braided stream deposits, Ph.D. Dissertation, Dept. of Geology, University of Wisconsin, Madison, 241 pp., 1992.

Yates, C.C., Analysis of Pumping Test Data of a Leaky and Layered Aquifer with Partially Penetrating Wells, M.Sc. Thesis, Dept. of Material Sciences and Mineral Engineering, University of California, Berkeley, 198 pp., 1988.

Table 1. Synthetic problem 1 inversions with $k = 2$, **b**'s only varying, and $E_{min} = 3.6$.

Case	Number of Forward Calculations	Number of Accepted Attractors	**P** ($\mathbf{b}_1$, $\mathbf{b}_2$)	E
1A	184	21	(0.29,0.47), (0.27,0.25)	3.2
1B	169	43	(0.20,0.20), (0.36,0.46)	2.8
1C	449	67	(0.36,0.46), (0.19,0.20)	0.3
1D	387	50	(0.21,0.21), (0.33,0.41)	1.5
1E	244	35	(0.19,0.18), (0.34,0.45)	1.7
1F	316	47	(0.28,0.26), (0.17,0.42)	3.4
Average‡	292	44	(0.22,0.22), (0.31,0.45)	2.2
Correct **P**			(0.35,0.45), (0.19,0.19)	10^{-10}
			(0.19,0.19), (0.35,0.45)	1.1
Uniform medium				46

CPU time per iteration is 10 sec on a Solbourne 500 series workstation
‡order of $\mathbf{b}_1$ and $\mathbf{b}_2$ interchanged for Cases A and C before average taken

Table 2. Synthetic problem 2 (high anomaly) inversions with $k = 3$, attractor points that increment properties, and $E_{min} = 1.6$.

Case	Number of Forward Calculations	Number of Accepted Attractors	E
2A	795	71	1.4
2B	87	20	1.6
2C	2,606	181	1.2
Uniform medium			92

CPU time per iteration is 17 sec on a Solbourne 500 series workstation

Table 3. Synthetic problem 2 (low anomaly) inversions with $k = 3$, attractor points that decrement properties, and $E_{min} = 1.6$.

Case	Number of Forward Calculations when Best Energy Found	Total Number of Forward Calculations	E
2K	2,929	3,497	8.4
2L	10,929	13,562	5.6
2M	5,271	26,164	3.9
Uniform medium			91

Table 4. Synthetic problem 2 inversions for various well locations. Three $k = 3$ inversions were done for each problem, using different random seeds. In all cases $E_{min} = 1.6$.

Well Locations	Anomaly	Number of Forward Calculations†	E
Outer	High	1,900-2,900	1.3-1.5
	Low	6,000-13,200	0.8-1.4
Inner	High	700-2,600	1.2-1.6
	Low	6,100-12,400	1.3-1.6
Random	High	1,100-2,100	0.9-1.6
Random‡	High	500-1,100	1.0-1.6

†Rounded to nearest hundred
‡Alternate pumping well, location shown in Figure 26.

Table 5. Kesterson Reservoir inversions with $k = 4$ and attractor points that decrement transmissivity.

Case	Number of Forward Calculations	Number of Accepted Attractors	E
K1	10,579	-	1.6
K2	14,993	349	2.1
K3	7,600	354	1.7
Uniform medium			25

CPU time per iteration is 77 sec on a Solbourne 500 series workstation

Table 6. Stripa H-zone C1-2 interference test inversions with $k = 4$ and attractor points that modify transmissivity and storativity.

Case	Mapping from Attractor to Lattice	Number of Forward Calculations when Best Energy Found	Total Number of Forward Calculations	Energy	SDE Flow Rate (10^{-6} m^3/s)
S1	Plus-minus	8,825	13,729	10	0.22
S2	Increment	10,453	10,710	8.7	0.13
S3	Decrement	7,166	11,457	19	0.38
Uniform Medium				51	0.36
Field Observation					0.21 ± 0.06

CPU time per iteration is 3.5 min on a Solbourne 500 series workstation

FIGURE CAPTIONS

Fig. 1. The effect of various affine transforms on a set of points.

Fig. 2. Generation of Sierpinski's gasket using an IFS with $k = 3$ and a set A_0 forming a cross.

Fig. 3. Generation of an attractor using an IFS with $k = 4$ and a set A_0 consisting of a single point.

Fig. 4. A sequence of attractors generated by IFS's with $k = 3$ whose parameters differ by a small amount. For the mth frame, $\mathbf{P}_m = \mathbf{P}_{m-1} + \Delta\mathbf{P}$, where $\Delta\mathbf{P}$ is a vector with random increments and $|\Delta\mathbf{P}| = 0.2$.

Fig. 5. The variation in attractor as parameters of the IFS change. For the mth frame in each series, $\mathbf{P}_m = \mathbf{P}_1 + \Delta\mathbf{P}_m$, where $\Delta\mathbf{P}_m$ is a vector with random increments.

Fig. 6. Schematic diagram of the mapping from attractor points to lattice element hydrologic properties. In the frame at the right, element thickness is proportional to transmissivity.

Fig. 7. Example of the mapping from attractor points to transmissivity distribution. Frame (a) shows the attractor superposed on the lattice, and frame (b) shows the transmissivity distribution, in which element thickness is proportional to T/T_0. The solid circles mark the well locations for synthetic problem 1.

Fig. 8. Transient drawdowns at the four observation wells for synthetic problem 1. The arrangement of the plots on the page follows the locations of the observation wells in the well field.

Fig. 9. Energy variation during the inversion for Case 1E. The minimum energy so far is shown as a dotted line in both frames.

Fig. 10. The final attractors for six inversions of synthetic problem 1, using IFS's with $k = 2$ with only the **b** terms of the affine transforms varying. Well locations are marked with open circles.

Fig. 11. The final attractors for six inversions of synthetic problem 1, using IFS's with $k = 2$ with all parameters of the affine transforms varying.

Fig. 12. The transmissivity distributions for the six inversions of synthetic problem 1. Element thickness is proportional to T/T_0.

Fig. 13. The mean transmissivity distribution for the six distributions shown in Figure 12, and the mean transmissivity distribution for 30 inversions all using the same parameters, but

different random seeds. Element thickness is proportional to T/T_0.

Fig. 14. A schematic diagram showing the regions of an aquifer in which heterogeneities tend to have the most affect on well-test results; these are the regions directly between pumping wells and observation wells.

Fig. 15. Model for synthetic problem 2, showing the lattice, well locations (solid circles), and the central square anomaly, which may have transmissivity and storativity either 100 times greater or 100 times less than the background values. The pumping well is the middle well on the left.

Fig. 16. Synthetic data at the five observation wells for synthetic problem 2, compared to the response for a uniform medium. The arrangement of the plots on the page follows the locations of the observation wells in the well field.

Fig. 17. The initial attractor for the $k = 3$ inversions of synthetic problem 2.

Fig. 18. Transient drawdowns for synthetic problem 2 with the high anomaly when attractor points increment properties.

Fig. 19. The final attractors for three $k = 3$ inversions of synthetic problem 2 with the high anomaly, when attractor points increment properties.

Fig. 20. The final attractors for three $k = 3$ inversions of synthetic problem 2 with the high anomaly, when attractor points decrement properties.

Fig. 21. The final attractors for two $k = 4$ inversions of synthetic problem 2 with the high anomaly, when attractor points decrement properties.

Fig. 22. Transient drawdowns for synthetic problem 2 with the high anomaly when attractor points decrement properties.

Fig. 23. The final attractor for a $k = 4$ inversion of synthetic problem 2 with the high anomaly, using the plus-minus algorithm. Attractor points which increment transmissivity and storativity are shown as pluses and points which decrement properties are shown as open circles. Only one quarter of the attractor points used are plotted (256 out of 1024), in order for the symbols to be more readily distinguishable.

Fig. 24. Transient drawdowns for synthetic problem 2 with the low anomaly when attractor points decrement properties.

Fig. 25. The final attractors for three $k = 3$ inversions of synthetic problem 2 with the low anomaly, when attractor points decrement properties.

Fig. 26. The well locations used for the inversions of synthetic problem 2, which are summarized in Table 4.

Fig. 27. The nested TRINET lattice used for the Kesterson inversion. Frame (a) shows the central portion of the lattice; the pumping well is at $x = 0$, $y = 0$, the locations of the observation wells are shown as solid circles. Frame (b) shows the entire lattice; head is held constant at $x = \pm 600$, $y = \pm 600$.

Fig. 28. Observed and calculated transient drawdowns for Kesterson. The arrangement of the plots on the page follows the locations of the observation wells in the well field.

Fig. 29. Results of three decremented-transmissivity inversions for Kesterson: top row – the final attractor for each case; middle row – the TRINET lattice plotted with element thickness proportional to transmissivity; bottom row – a grey-scale plot of effective aquifer transmissivity $\tilde{T}$. The minimum transmissivity level shown is $T_0/100$, although several elements have even lower T values.

Fig. 30. The final attractors for the incremented-transmissivity inversions for Kesterson.

Fig. 31. The central portion of the nested TRINET lattice used for the Stripa inversion.

Fig. 32. Observed and calculated transient drawdowns for the Stripa C1-2 interference test for Case S1. The arrangement of the plots on the page shows the locations where the boreholes intersect the H-zone.

Fig. 33. Energy variation during the inversion of the Stripa C1-2 interference test for Case S1. The minimum energy so far is shown in both frames.

Fig. 34. Results of three inversions for the Stripa C1-2 interference test: top row – the final attractor for each case; middle row – the TRINET lattice plotted with element thickness proportional to transmissivity; bottom row – a grey-scale plot of effective aquifer transmissivity $\tilde{T}$. For Case S1 attractor points which increment properties are shown as pluses and points which decrement properties are shown as open circles. For Case S2 attractor points increment properties and for Case S3 points decrement properties. The range of transmissivity levels shown is $T_0/100$ to $40T_0$, although several elements have more extreme values.

Fig. A.1. The variation in attractor as parameters of the IFS change, using the rotation-matrix form for $\mathbf{B}$, Equation (A.1). For the mth frame $\mathbf{P}_m = \mathbf{P}_1 + \Delta\mathbf{P}_m$, where $\Delta\mathbf{P}_m$ is a vector with random increments and $|\Delta\mathbf{P}_m| = 0.4$.

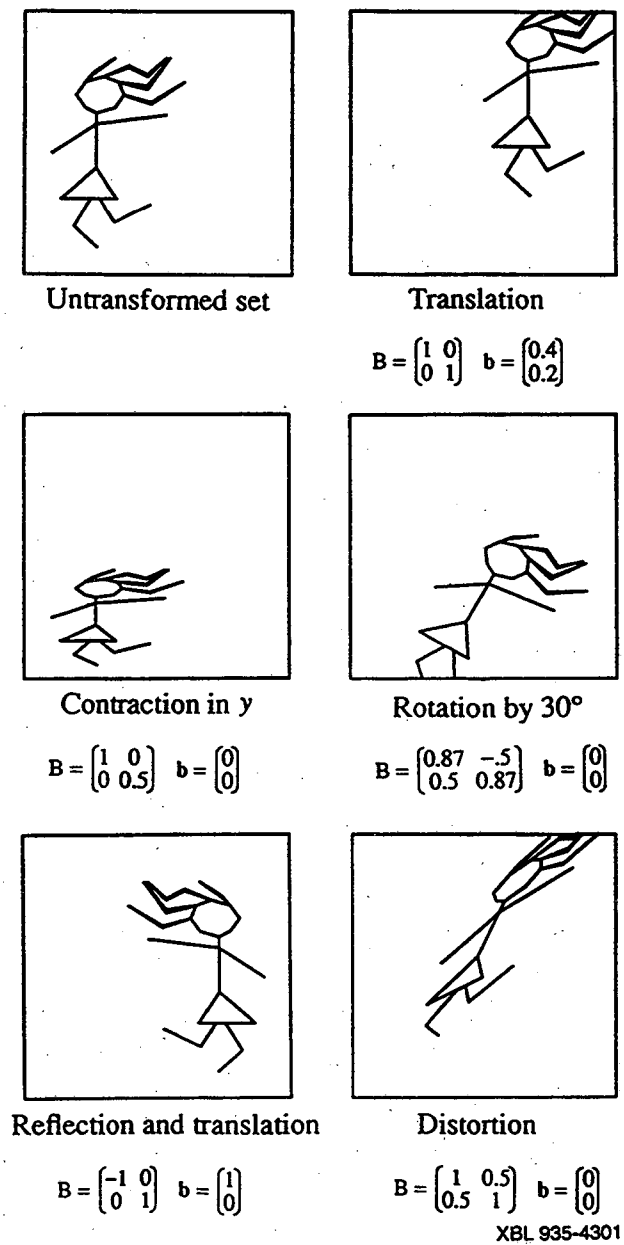

Fig. 1. The effect of various affine transformations on a set of points.

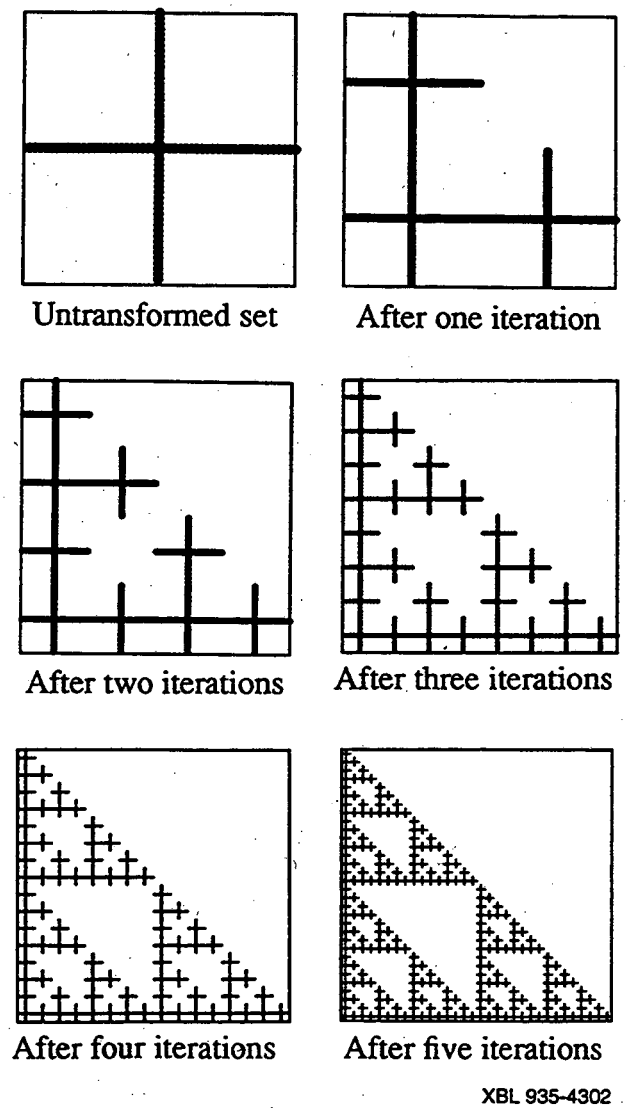

Fig. 2. Generation of Sierpinski's gasket using an IFS with $k = 3$ and a set A_0 forming a cross.

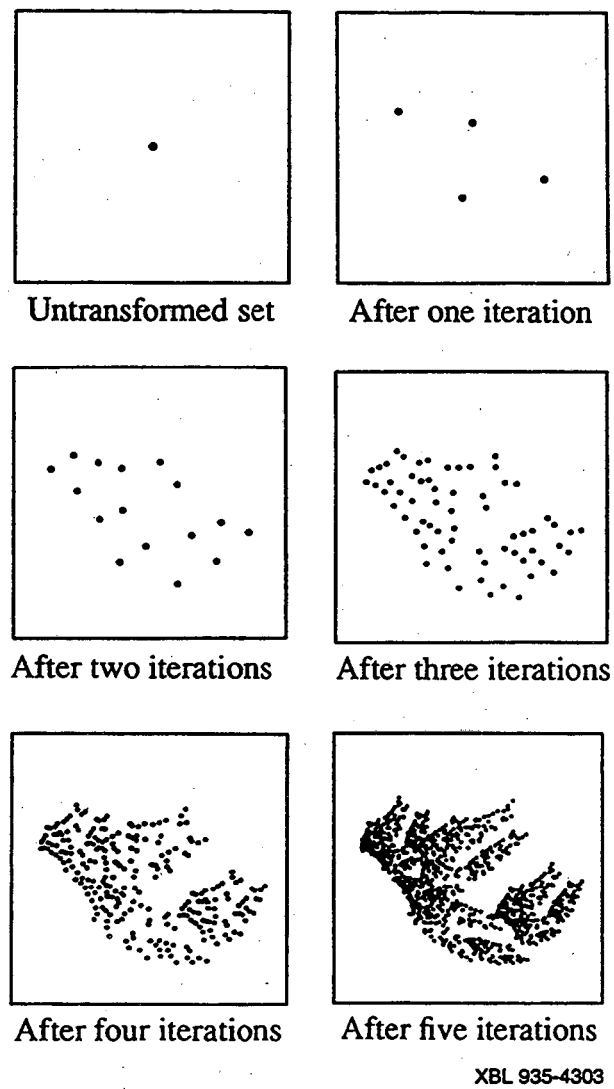

Fig. 3. Generation of an attractor using an IFS with $k = 4$ and a set A_0 consisting of a single point.

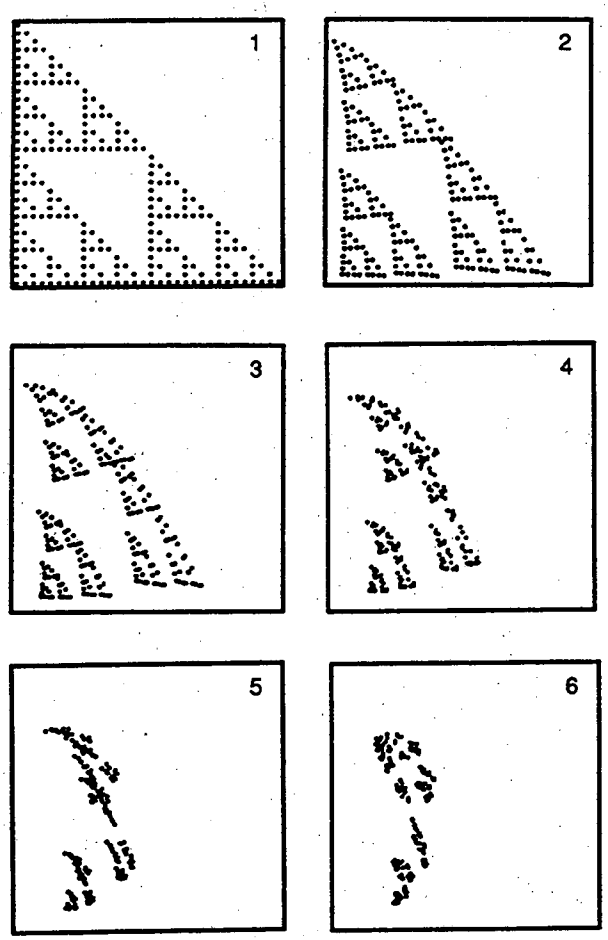

XBL 935-4304

Fig. 4. A sequence of attractors generated by IFS's with $k = 3$ whose parameters differ by a small amount. For the m th frame, $\mathbf{P}_m = \mathbf{P}_{m-1} + \Delta\mathbf{P}$, where $\Delta\mathbf{P}$ is a vector with random increments and $|\Delta\mathbf{P}| = 0.2$.

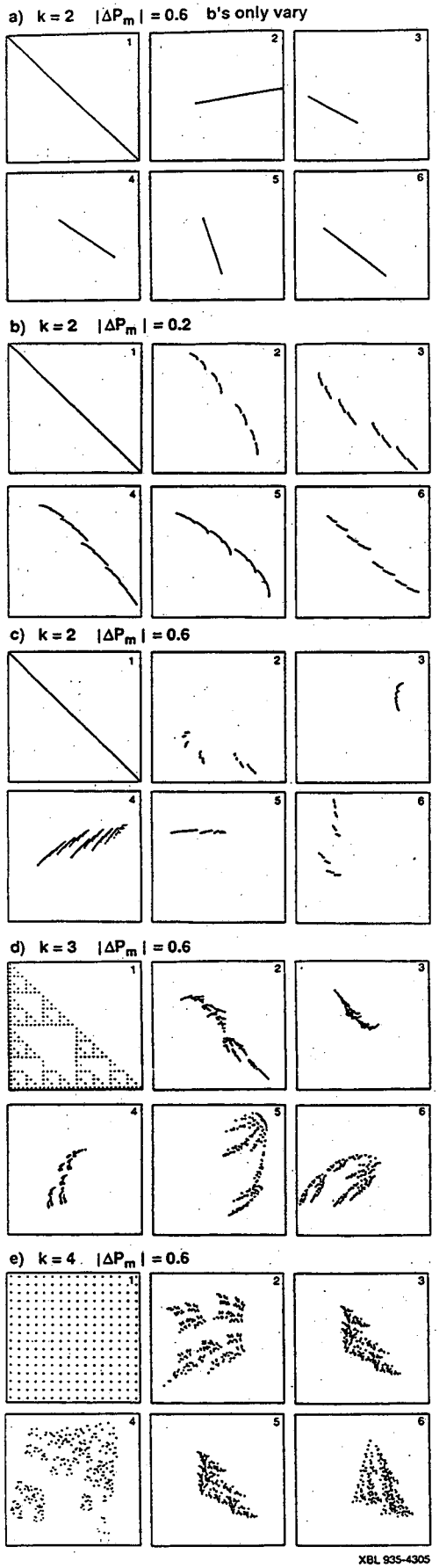

Fig. 5. The variation in attractor as parameters of the IFS change. For the m th frame in each series, $\mathbf{P}_m = \mathbf{P}_1 + \Delta\mathbf{P}_m$, where $\Delta\mathbf{P}_m$ is a vector with random increments.

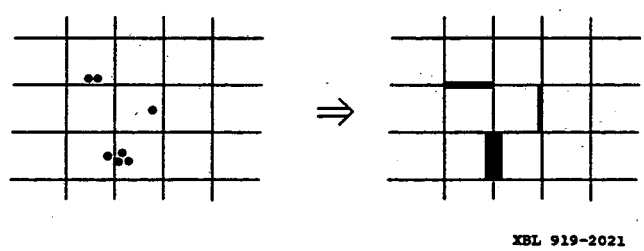

Fig. 6. Schematic diagram of the mapping from attractor points to lattice element hydrologic properties. In the frame at the right, element thickness is proportional to transmissivity.

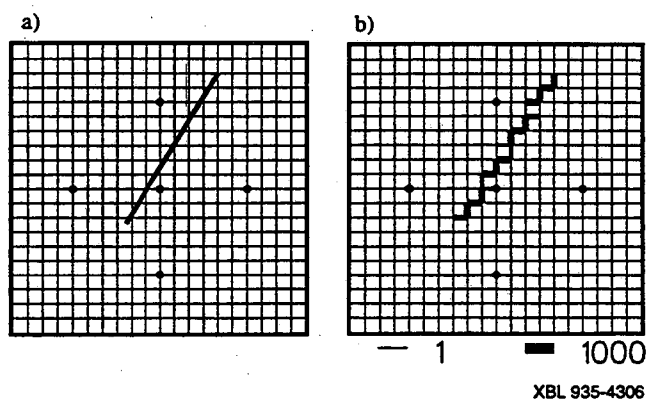

Fig. 7. Example of the mapping from attractor points to transmissivity distribution. Frame (a) shows the attractor superposed on the lattice, and frame (b) shows the transmissivity distribution, in which element thickness is proportional to T/T_0. The solid circles mark the well locations for synthetic problem 1.

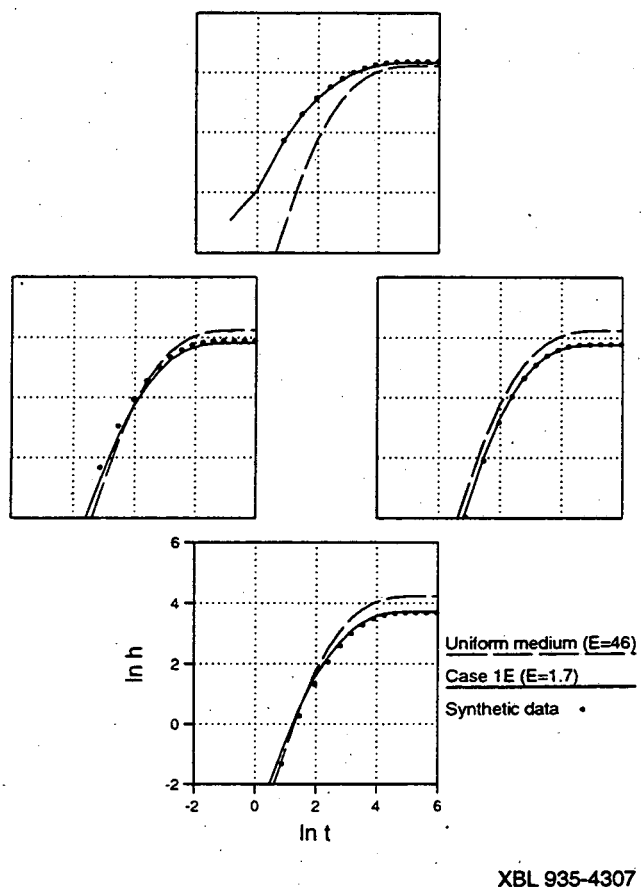

Fig. 8. Transient drawdowns at the four observation wells for synthetic problem 1. The arrangement of the plots on the page follows the locations of the observations wells in the well field.

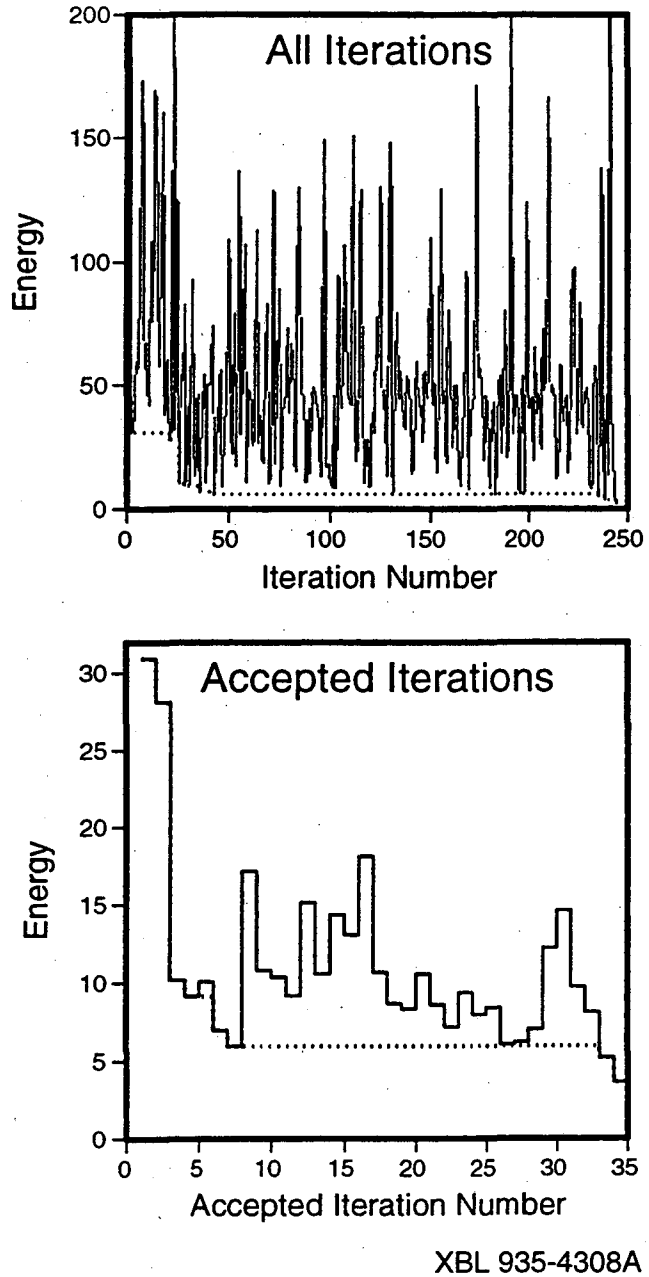

Fig. 9. Energy variation during the inversion for Case 1E. The minimum energy so far is shown as a dotted line in both frames.

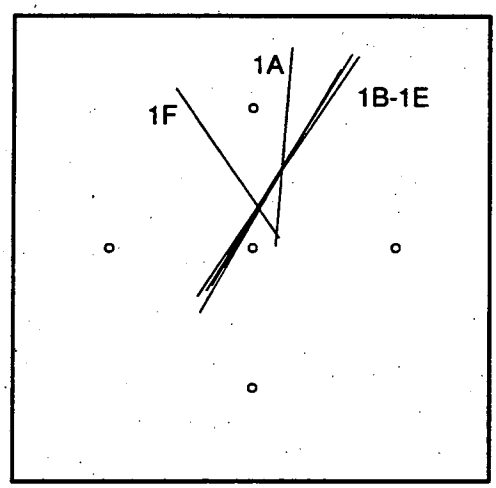

XBL 935-4309

Fig. 10. The final attractors for six inversions of synthetic problem 1, using IFS's with $k = 2$ with only the **b** terms of the affine transforms varying. Well locations are marked with open circles.

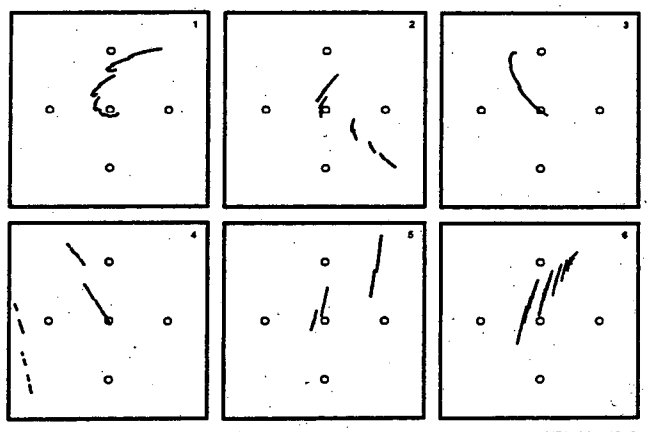

XBL 935-4310

Fig. 11. The final attractors for six inversions of synthetic problem 1, using IFS's with $k = 2$ with all parameters of the affine transforms varying.

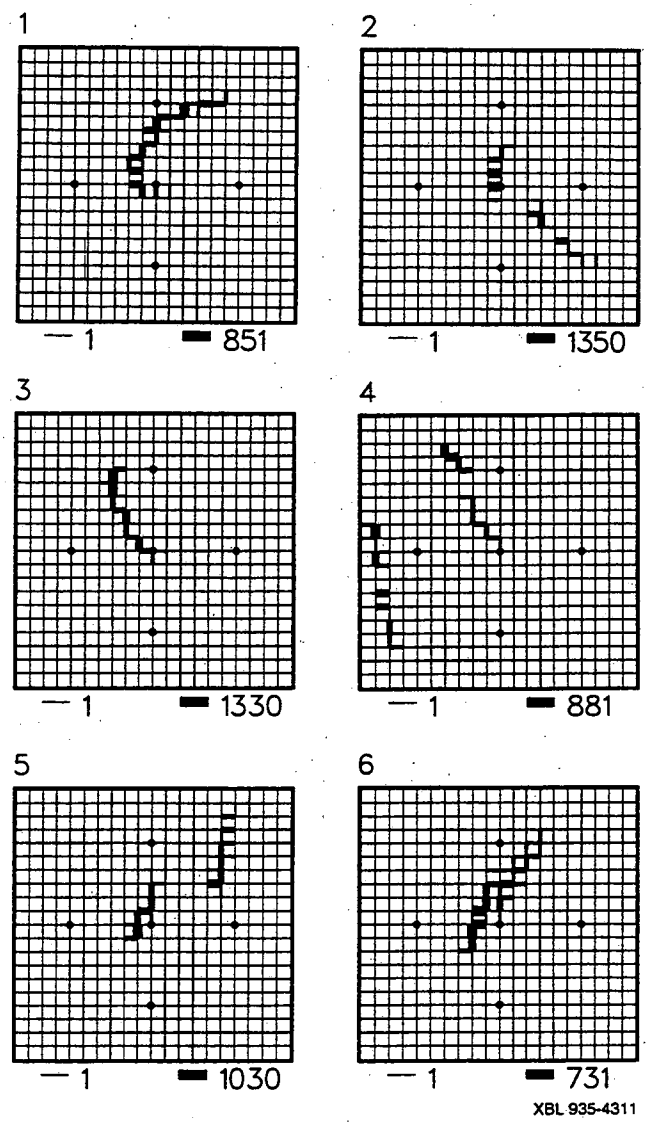

Fig. 12. The transmissivity distributions for the six inversions of synthetic problem 1. Element thickness is proportional to T/T_0.

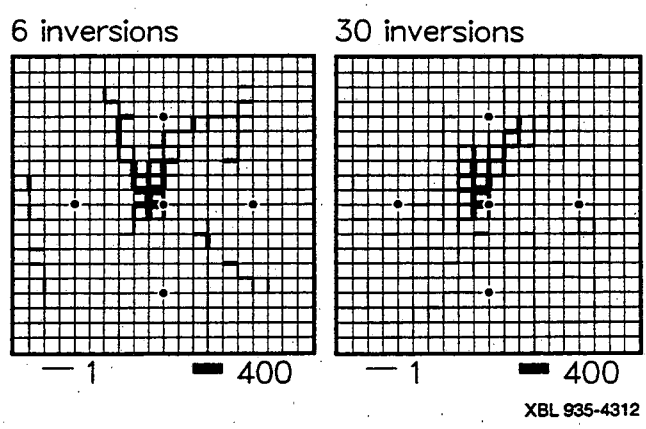

Fig. 13. The mean transmissivity distribution for the six distributions shown in Figure 12, and the mean transmissivity distribution for 30 inversions all using the same parameters, but different random seeds. Element thickness is proportional to T/T_0.

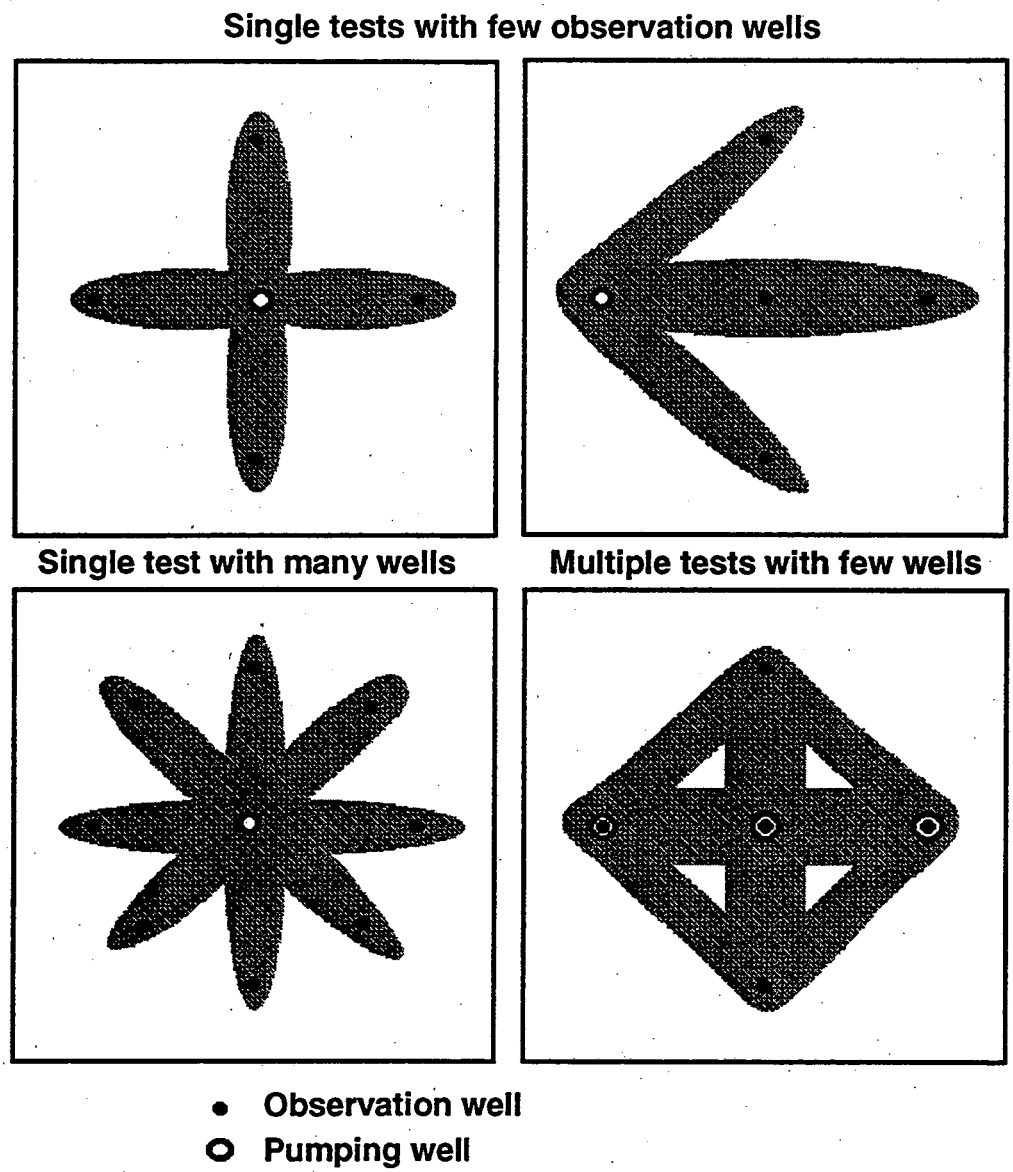

XBL 935-4313

Fig. 14. A schematic diagram showing the regions of an aquifer in which heterogeneities tend to have the most affect on well-test results; these are the regions directly between pumping wells and observation wells.

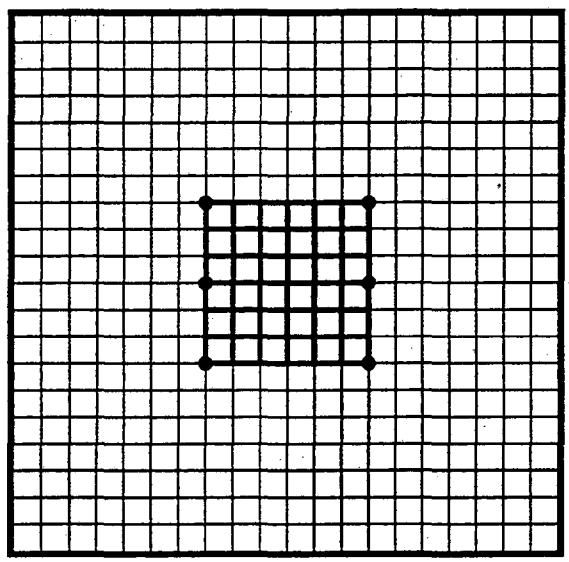

XBL 935-4314

Fig. 15. Model for synthetic problem 2, showing the lattice, well locations (solid circles), and the central square anomaly, which may have transmissivity and storativity either 100 times greater or 100 times less than the background values. The pumping well is the middle well on the left.

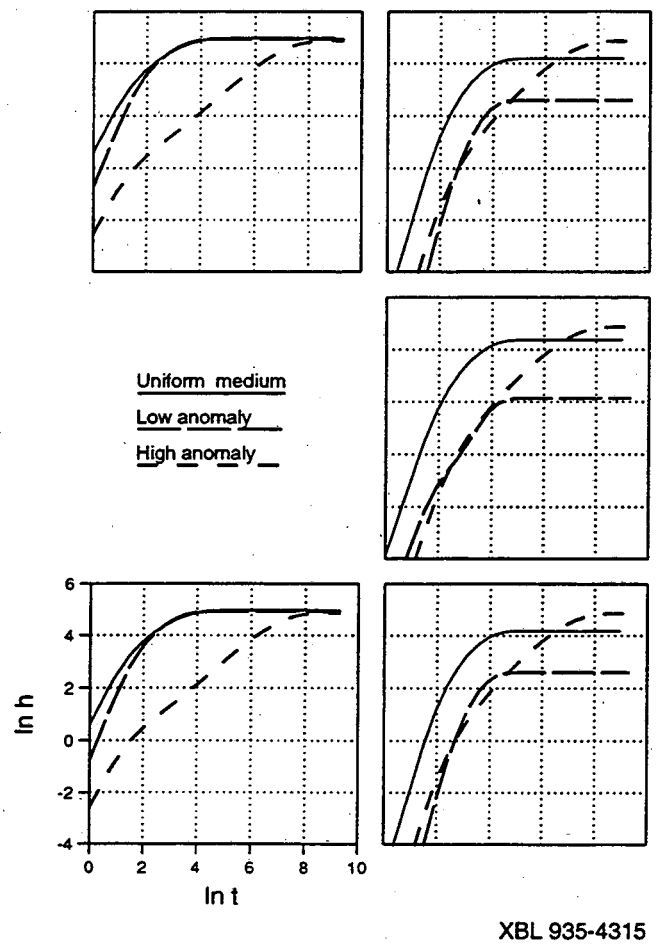

Fig. 16. Synthetic data at the five observation wells for synthetic problem 2, compared to the response for a uniform medium. The arrangement of the plots on the page follows the locations of the observation wells in the well field.

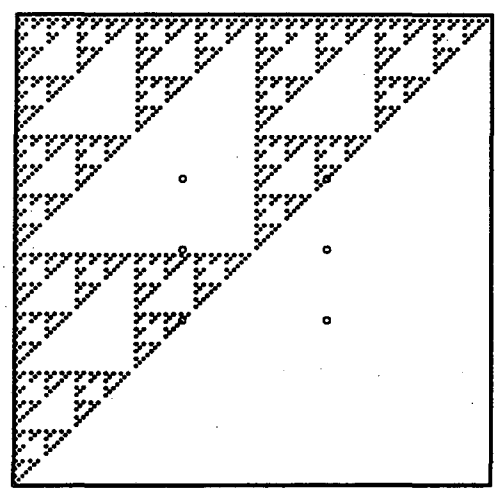

XBL 935-4316

Fig. 17. The initial attractor for the $k = 3$ inversions of synthetic problem 2.

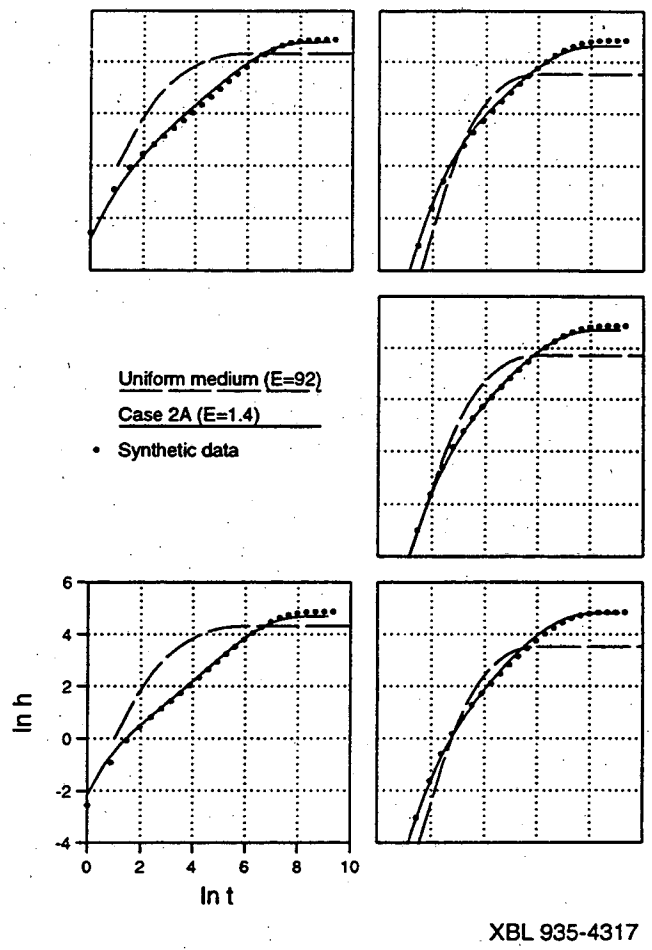

Fig. 18. Transient drawdowns for the synthetic problem 2 with the high anomaly when attractor points increment properties.

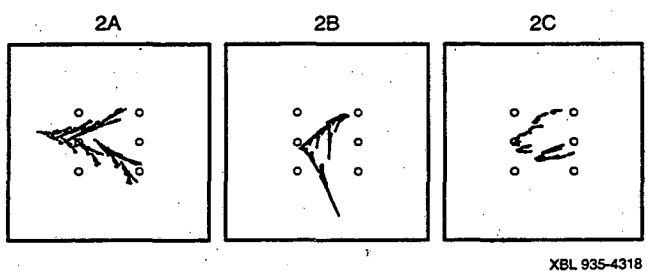

Fig. 19. The final attractors for three $k = 3$ inversions of synthetic problem 2 with the high anomaly, when attractor points increment properties.

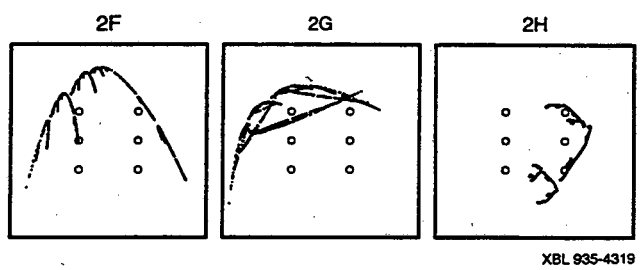

Fig. 20. The final attractors for three $k = 3$ inversions of synthetic problem 2 with the high anomaly, when attractor points decrement properties.

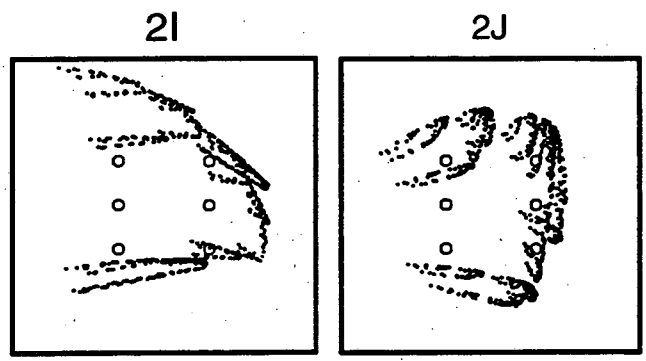

XBL 935-4320

Fig. 21. The final attractors for two $k = 4$ inversions of synthetic problem 2 with the high anomaly, when attractor points decrement properties.

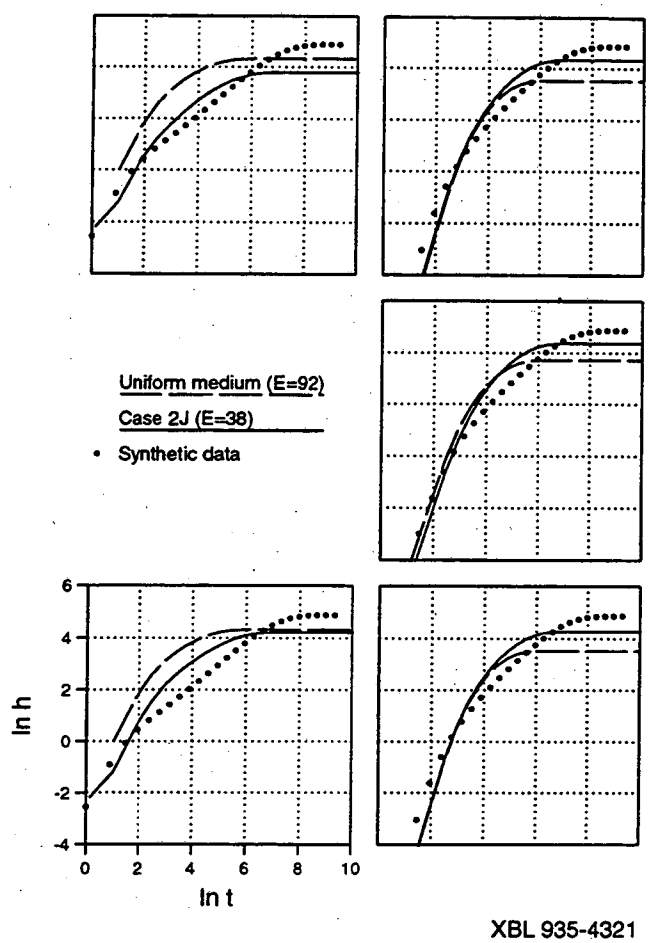

Fig. 22. Transient drawdowns for synthetic problem 2 with the high anomaly when attractor points decrement properties.

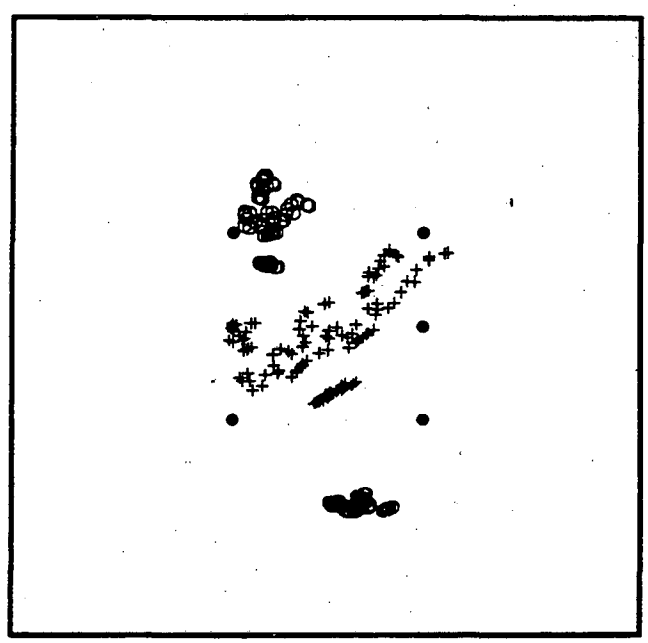

XBL 935-4322A

Fig. 23. The final attractor for a $k = 4$ inversion of synthetic problem 2 with the high anomaly, using the plus-minus algorithm. Attractor points which increment transmissivity and storativity are shown as pluses and points which decrement properties are shown as open circles. Only one quarter of the attractor points used are plotted (256 out of 1024), in order for the symbols to be more readily distinguishable.

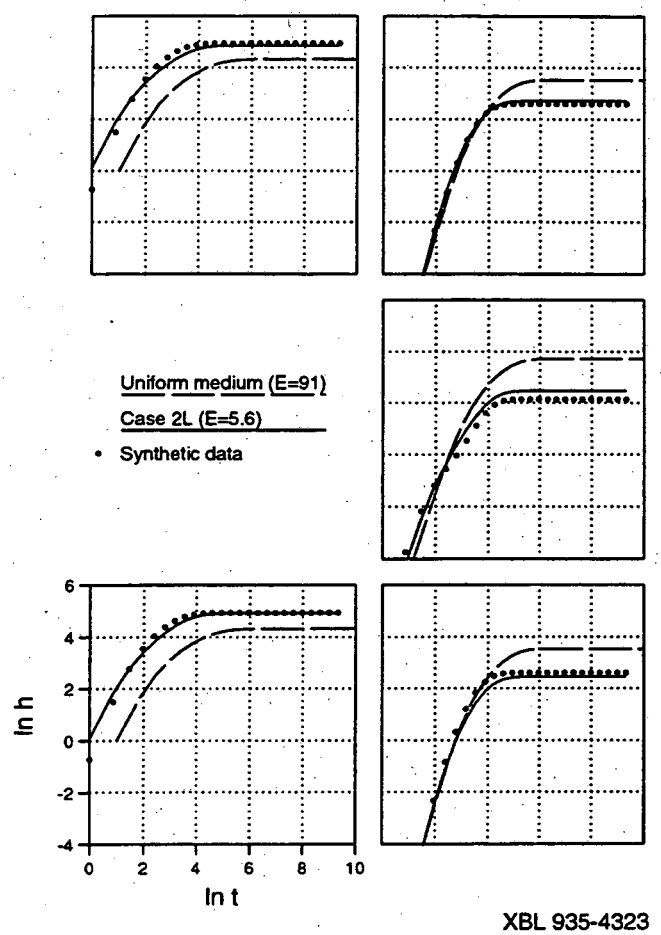

Fig. 24. Transient drawdowns for synthetic problem 2 with the low anomaly when attractor points decrement properties.

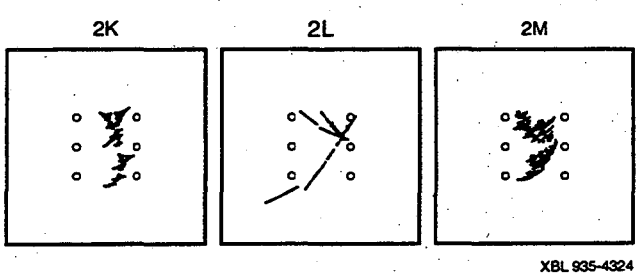

Fig. 25. The final attractors for three $k = 3$ inversions of synthetic problem 2 with the low anomaly, when attractor points decrement properties.

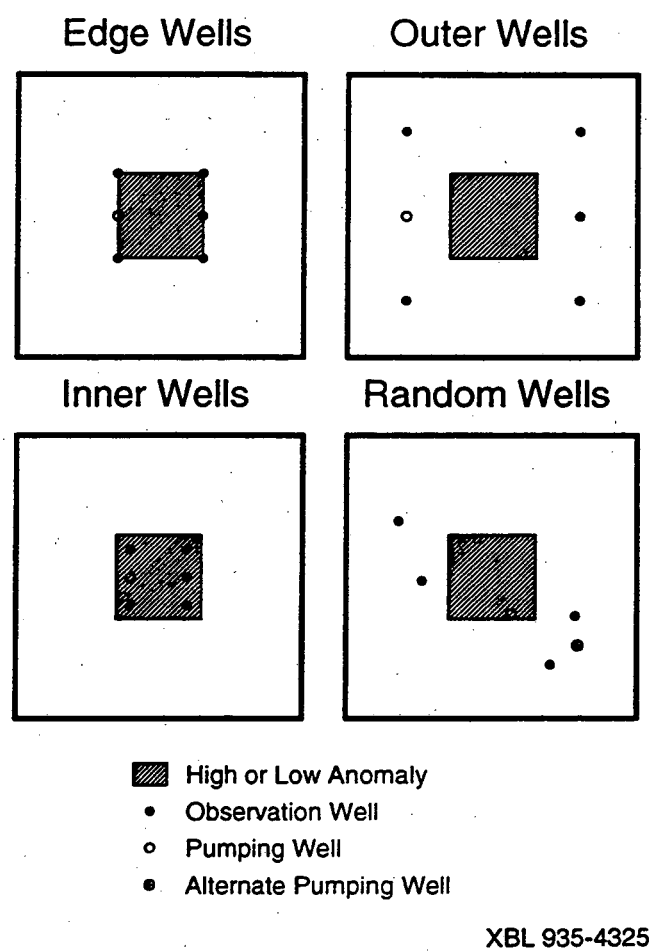

Fig. 26. The well locations used for the inversions of synthetic problem 2, which are summarized in Table 4.

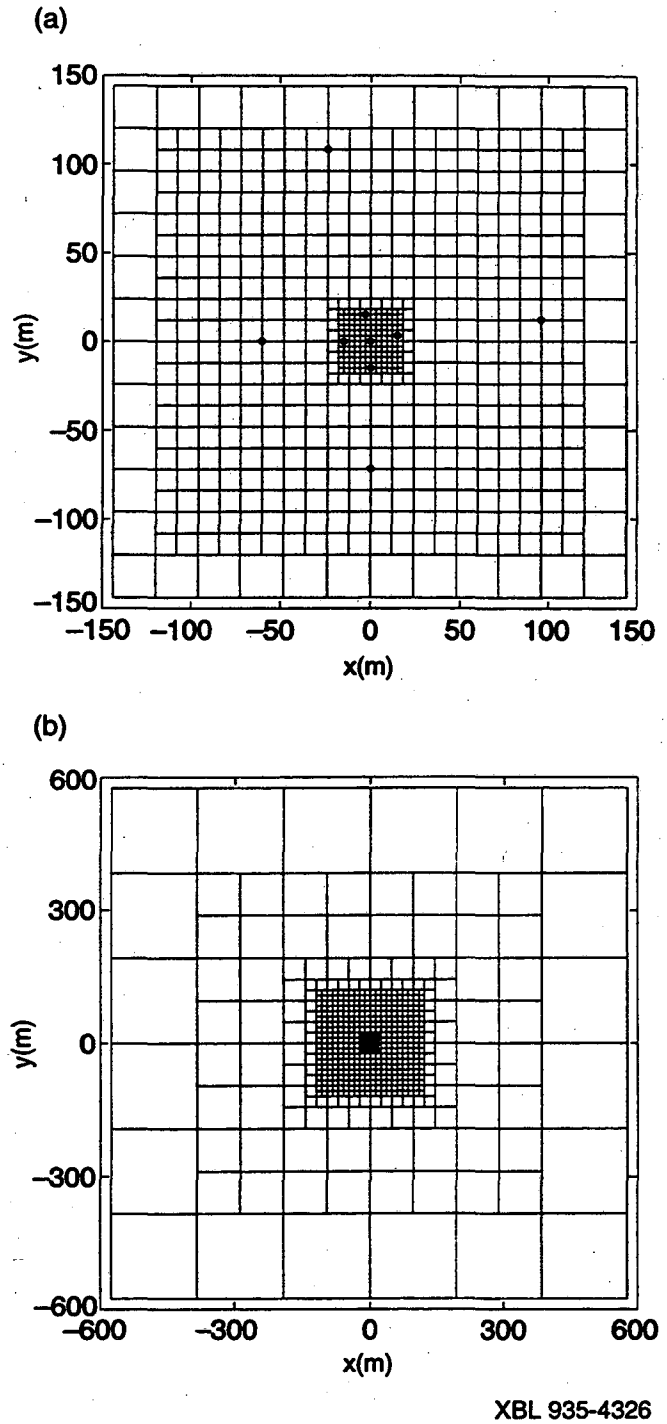

Fig. 27. The nested TRINET lattice used for the Kesterson inversion. Frame (a) shows the central portion of the lattice; the pumping well is at $x = 0$, $y = 0$, the locations of the observation wells are shown as solid circles. Frame (b) shows the entire lattice; head is held constant at $x = \pm 600$, $y = \pm 600$.

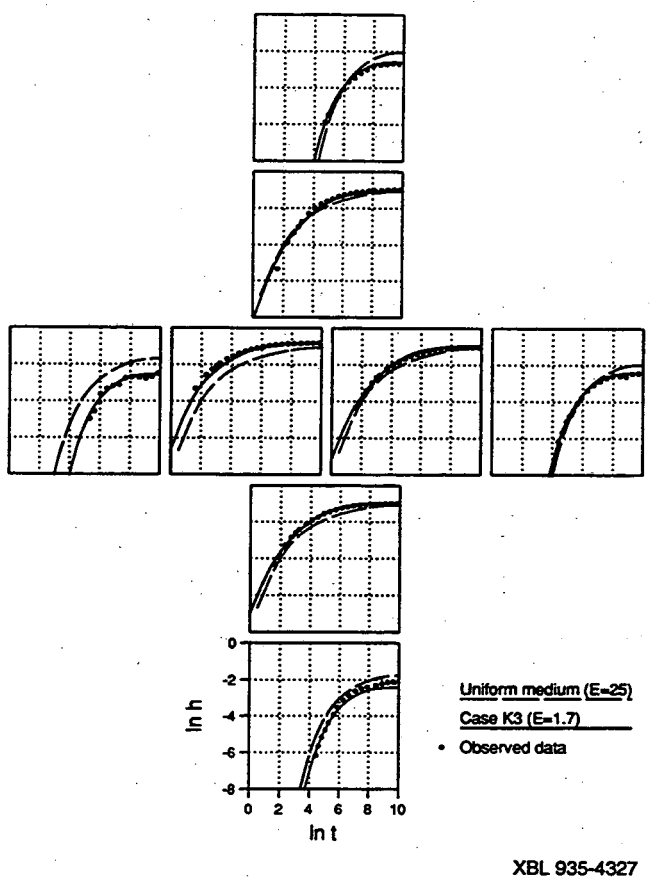

Fig. 28. Observed and calculated transient drawdowns for Kesterson. The arrangement of the plots on the page follows the locations of the observation wells in the well field.

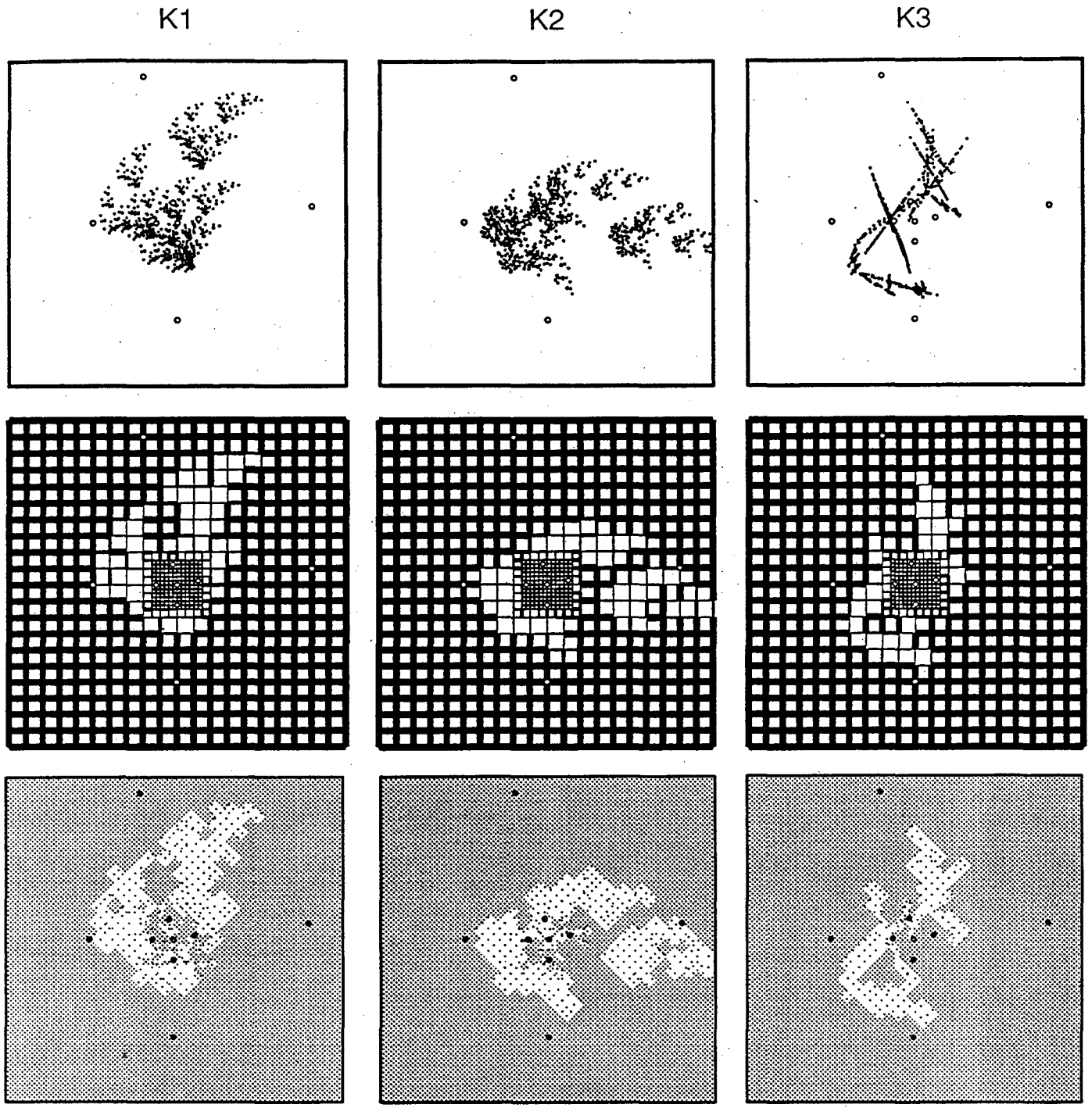

Fig. 29. Results of three decremented-transmissivity inversions for Kesterson: top row – the final attractor for each case; middle row – the TRINET lattice plotted with element thickness proportional to transmissivity; bottom row – a grey-scale plot of effective aquifer transmissivity $\tilde{T}$. The minimum transmissivity level shown is $T_0/100$, although several elements have even lower T values.

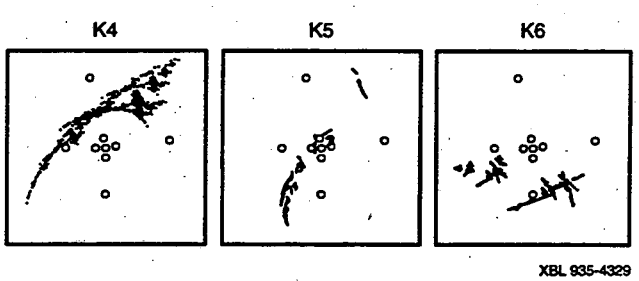

Fig. 30. The final attractors for the incremented-transmissivity inversions for Kesterson.

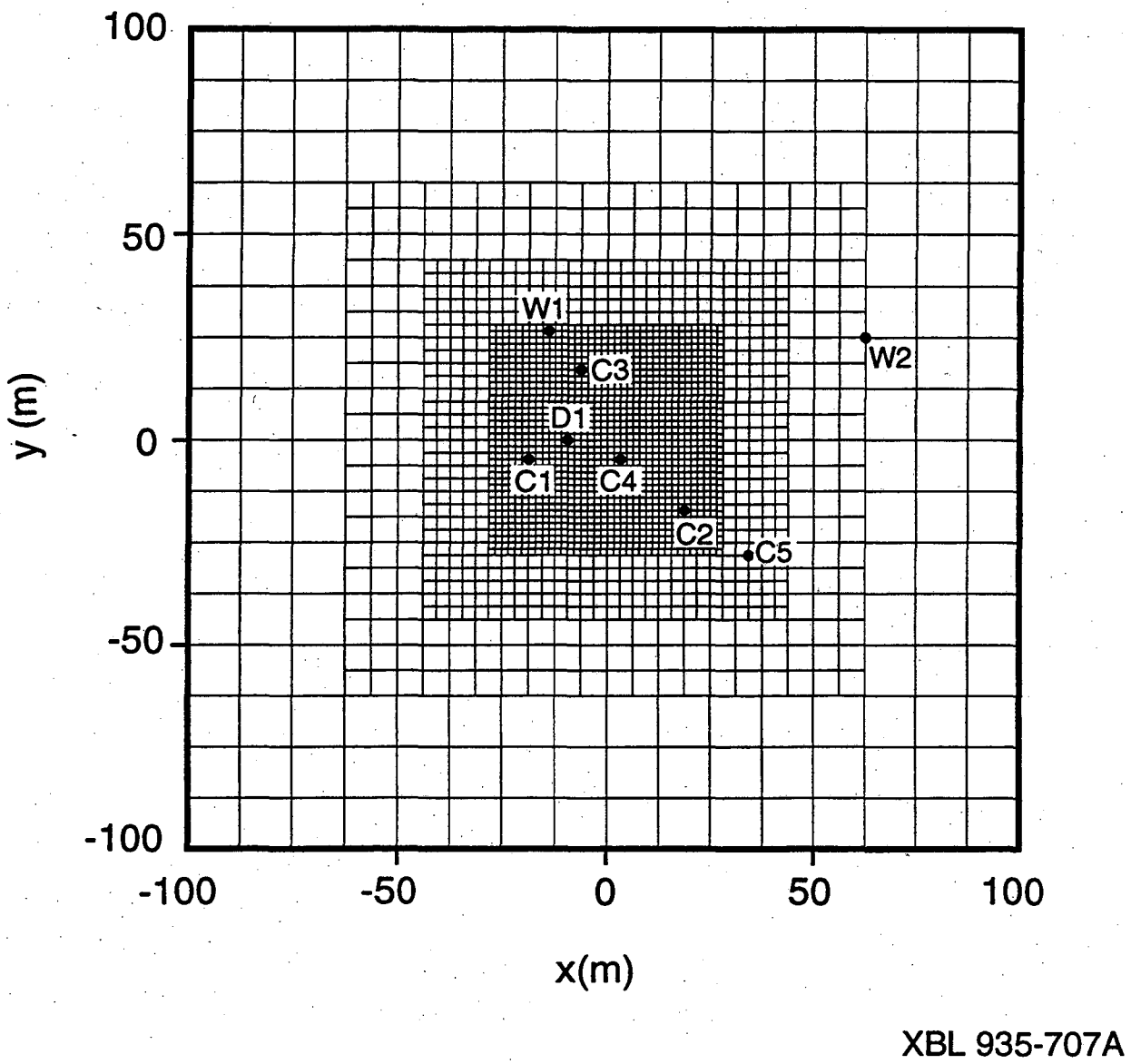

Fig. 31. The central portion of the nested TRINET lattice used for the Stripa inversion.

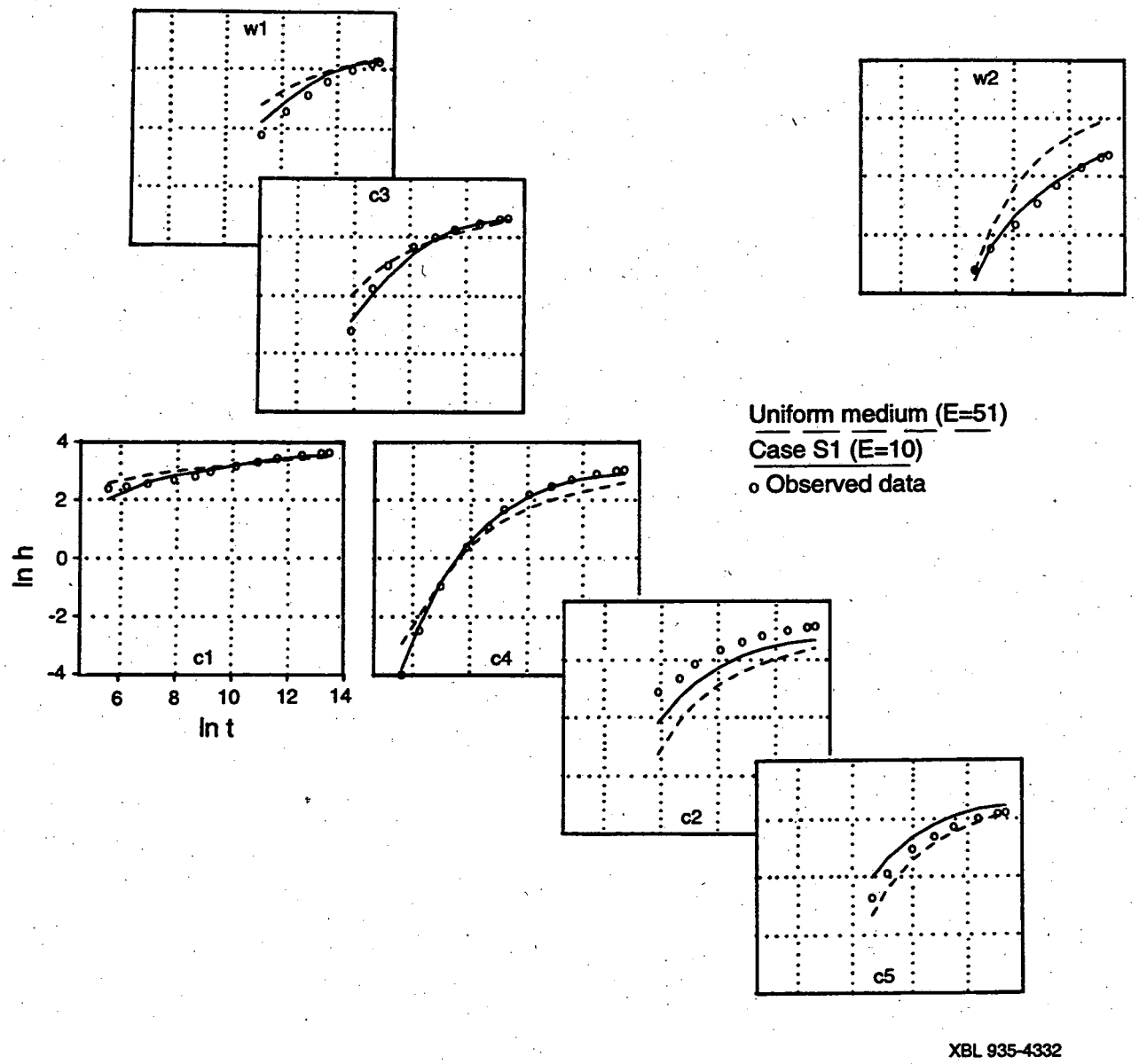

Fig. 32. Observed and calculated transient drawdowns for the Stripa C1-2 interference test for Case S1. The arrangement of the plots on the page shows the locations where the boreholes intersect the H-zone.

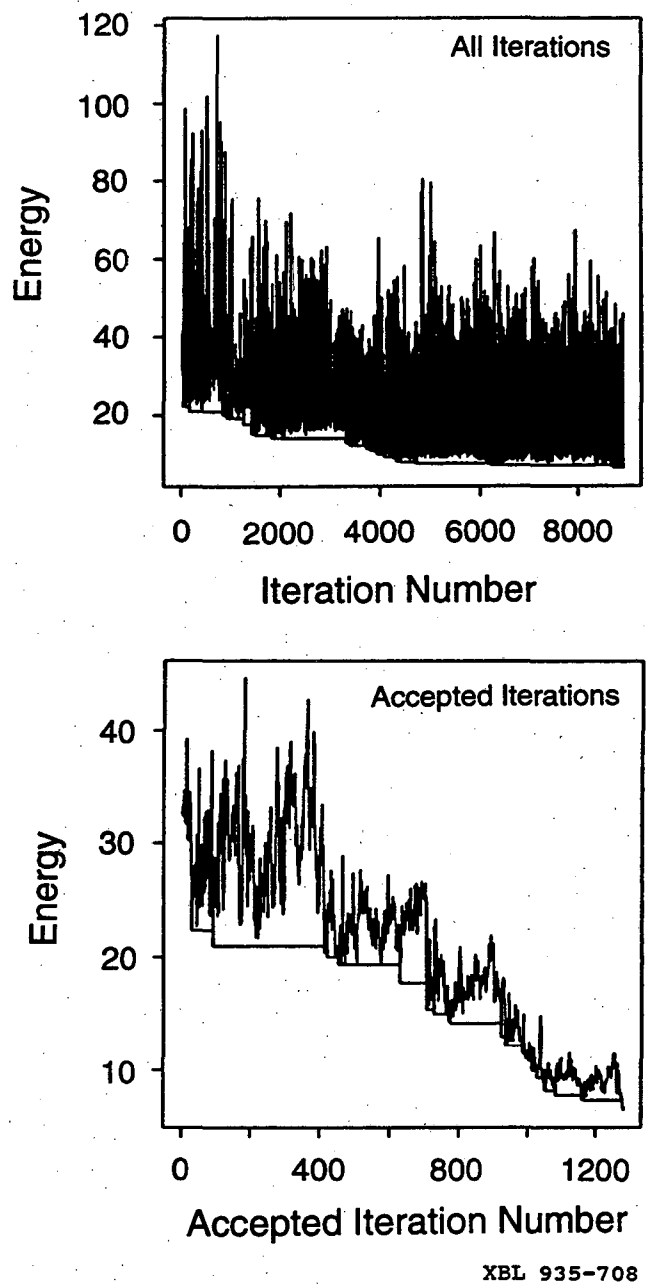

Fig. 33. Energy variation during the inversion of the Stripa C1-2 interference test for Case S1. The minimum energy so far is shown in both frames.

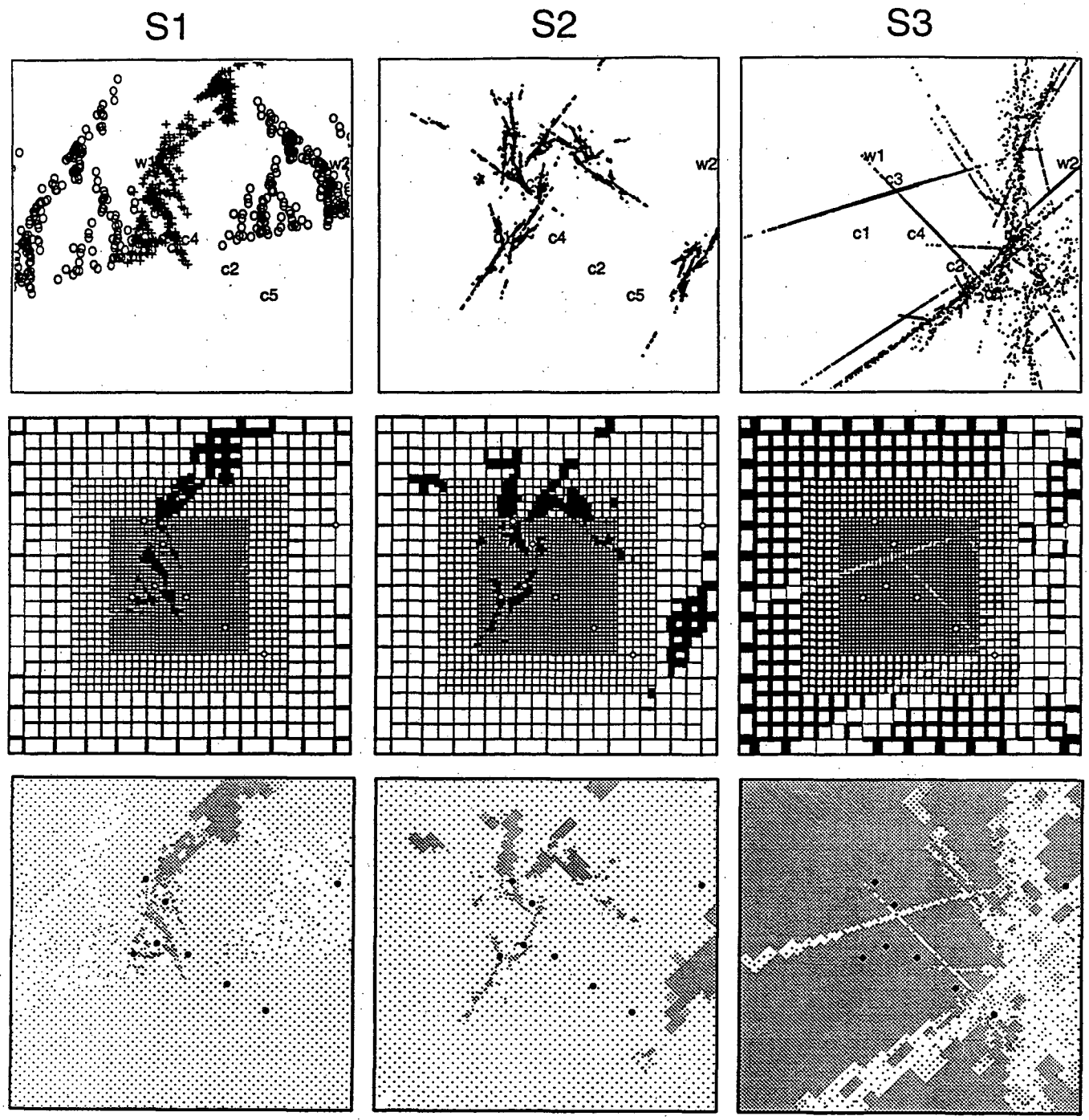

Fig. 34. Results of three inversions for the Stripa C1-2 interference test: top row – the final attractor for each case; middle row – the TRINET lattice plotted with element thickness proportional to transmissivity; bottom row – a grey-scale plot of effective aquifer transmissivity $\bar{T}$. For Case S1 attractor points which increment properties are shown as pluses and points which decrement properties are shown as open circles. For Case S2 attractor points increment properties and for Case S3 points decrement properties. The range of transmissivity levels shown is $T_0/100$ to $40T_0$, although several elements have more extreme values.

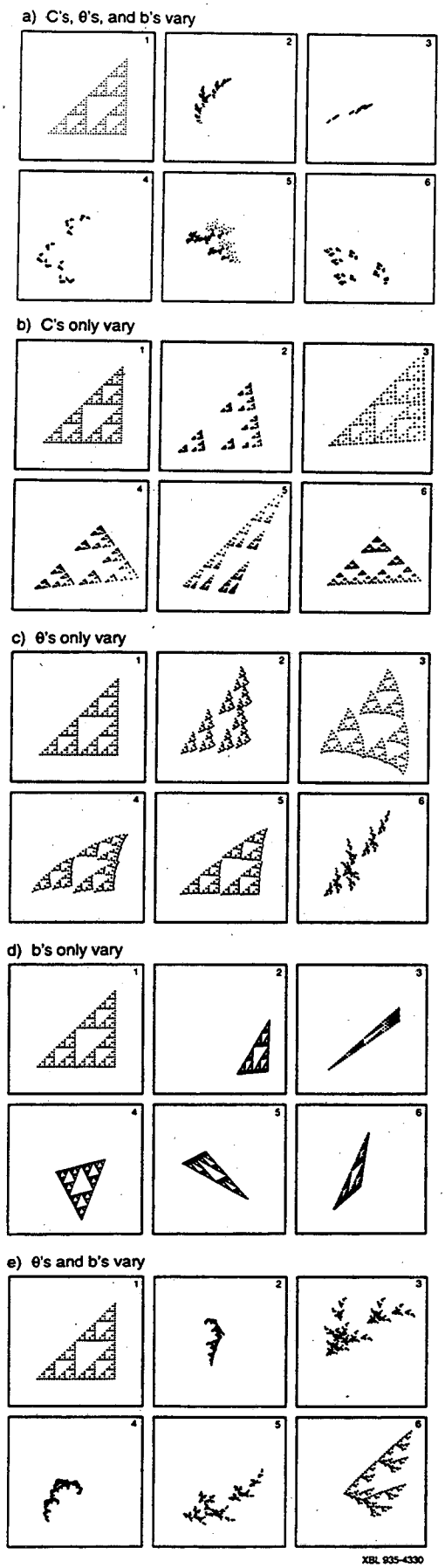

Fig. A1. The variation in attractor as parameters of the IFS change, using the rotation-matrix form for **B**, Equation (A.1). For the m th frame $\mathbf{P}_m = \mathbf{P}_1 + \Delta\mathbf{P}_m$, where $\Delta\mathbf{P}_m$ is a vector with random increments and $|\Delta\mathbf{P}_m| = 0.4$.

LAWRENCE BERKELEY LABORATORY
UNIVERSITY OF CALIFORNIA
TECHNICAL INFORMATION DEPARTMENT
BERKELEY, CALIFORNIA 94720